Synthesis of Cu-Doped ZnO/Ag/CuO Heterostructure: The Charge Transfer and Synergetic Effect on Anti-bacterial Activity and Methylene Blue Dye Degradation

Bontu Kefale

A Thesis Submitted to The Department of Applied Chemistry
School of Applied Natural Science

In Partial Fulfillment for the Degree of Master of Science in Applied Chemistry (Analytical Chemistry)

Office of Graduate Studies
Adama Science and Technology University

June, 2024
Adama, Ethiopia

Synthesis of Cu-Doped ZnO/Ag/CuO Heterostructure: The Charge Transfer and Synergetic Effect on Anti-bacterial Activity and Methylene Blue Dye Degradation

Bontu Kefale

Supervisors

Main supervisor: Buzuayehu Abebe (Ph.D.)

Co-supervisor: Dereje Tsagaye (Ph.D.)

A Thesis Submitted to the department of Applied Chemistry

School of Applied Natural Science

Office of Graduate Studies

Adama Science and Technology University

June, 2024

Adama, Ethiopia

Declaration

I declare that this master's thesis entitled "**Synthesis of Cu-Doped ZnO/Ag/CuO Heterostructure: The Charge Transfer and Synergetic effect on Anti-bacterial Activity and Methylene Blue Dye Degradation**" is my work and has not been submitted to any university for similar purposes. The references used in this proposal are duly recognized by proper citation.

_____	_____	_____
Name of student	Signature	Date

Recommendation

We, the major and co-advisors of this thesis work, hereby certify that we have closely advised the student while developing this thesis and have read the draft thesis entitled "**Synthesis of Cu-Doped ZnO/Ag/CuO Heterostructure: The Charge Transfer and Synergetic effect on Anti-bacterial Activity and Methylene Blue Dye Degradation**" prepared under our guidance by Bontu Kefale. Therefore, we recommend the submission of the thesis paper to the department for further review and evaluation.

_____	_____	_____
Major Advisor	Signature	Date
_____	_____	_____
Co-advisor	Signature	Date

Approval

The advisors hereby certify that the recommendation and suggestions given by the Thesis review committee are appropriately incorporated into the final thesis entitled "**Synthesis of Cu-Doped ZnO/Ag/CuO Heterostructure: The Charge Transfer and Synergetic effect on Anti-bacterial Activity and Methylene Blue Dye Degradation**" By Bontu Kefale.

_____	_____	_____
Major Advisor	Signature	Date
_____	_____	_____
Co-advisor	Signature	Date

Approval of Board of Examiners

We, the undersigned, members of the Board of Examiners of the Thesis open defense by Bontu Kefale have read and evaluated the thesis entitled **"Synthesis of Cu-Doped ZnO/Ag/CuO Heterostructure: The Charge Transfer and Synergetic effect on Anti-bacterial Activity and Methylene Blue Dye Degradation**" and examined the candidate during the open defense. This is, therefore, to certify that the thesis is accepted for partial fulfillment of the requirement of the degree of Master of Science in Analytical Chemistry.

_____	_____	_____
Chairperson	Signature	Date
_____	_____	_____
Internal Examiner	Signature	Date
_____	_____	_____
External Examiner	Signature	Date

Final approval and acceptance of the thesis is contingent upon submission of its final copy to the Office of Postgraduate Studies (OPGS) through the Department Graduate Council (DGC) and School Graduate Committee (SGC).

_____	_____	_____
Department Head	Signature	Date
_____	_____	_____
School Dean	Signature	Date
_____	_____	_____
Office of Postgraduate Studies, Dean	Signature	Date

Acknowledgments

First and foremost, I would like to thank Almighty God for taking care of my life in all situations I have passed through and shaping my ways. To him alone, I ascribe all the glory. I sincerely acknowledge my hard-working advisors, Dr. Buzuayehu Abebe for his crucial remarks, valuable support, sustainable and appreciable guidance, and comments in every step of this work and Co-advisor Dr. Dereje Tsegaye for strong support, guidance, and encouragement throughout my study and during the write-up of this thesis. I appreciate the time they devoted to this work and their experience. It is a great privilege and honor for me to be advised by them. I would also to say thanks to lab Assistant Mr. Guta Amenu for his encouragement and support. I am enormously indebted to Adama Science and Technology University for sponsoring me to study for a master's degree. Also I would like to say thank you Applied Chemistry Department and Material Science and Engineering for their endless support. Last but not least, I would like to extend my most profound gratitude to all my family, relatives and friends for their sincere love, help, and encouragement during the entire study period

Table of contents

List of Figures

List of Table

List of Acronyms and Abbreviation

AOP	Advanced Oxidative Process
BUC	Bottom-up Combustion
CNT	Classical Nucleation Theory
DBPs	Disinfection by-products
DRS	Differential Reflectance Spectroscopy
FT-IR	Fourier Transform Infrared Spectroscopy
HSAB	Hard-Soft Acid Base
MB-D	Methylene Blue Dye
MHB	Muller Hinton Broth
PNCs	Pre-nucleation Clusters
PL	Photoluminescence
ROS	Reactive Oxygen Species
SCS	Solution Combustion Synthesis
SEM-EDX	Scanning Electron Microscopy-Energy Dispersive X-ray
TEM	Transmission Electron Microscopy
TGA	Thermogravimetric Analysis
UV-vis-DRS	Ultraviolet–visible Diffraction Spectroscopy
XAS	X-ray Absorption Spectroscopy
XRD	X-ray Diffraction

Abstract

It is observed that doped semiconductor heterostructures exhibit better properties than the separate constituents from which they are formed. In this work synthesis of porous structures using the bottom-up combustion (BUC) approach and effects of doping and heterojunction on charge transfer and visible light harvesting properties were studied. porous materials was produced using BUC approach as a result of gaseous by-products being removed. The XRD-based optimization showed that 1.00 g of PVA, 50 °C synthesis temperature, and 1 hour calcination time were obtained to be the optima. The XRD spectra analysis also showed the material's crystalline nature. The HR-TEM images and XRD patterns also confirm the formation of Cu-doped ZnO and ZnO/Ag/CuO (c-zac) heterostructures. The c-zac also has better optoelectrical and charge transfer properties than single ZnO. The c-zac heterostructure showed improved photocatalytic potential ($k = 0.067\ min^{-1}$) compared to single ZnO ($k = 0.0041\ min^{-1}$). This photocatalysis potential is associated with improved light absorption and charge transfer properties. The extended visible light absorption is due to the copper doping and surface plasmon resonance properties of silver. Antibacterial efficacy of the bottom-up combustion synthesized (uncalcined and calcined) ZnO and c-zac against bacterial pathogens was also assessed. The c-zac NCs exhibited broad spectrum activities against Streptococcus Pyogenes, with inhibition zone of 17.5 ±0.7mm. Least activity was seen against E-coli with inhibition zone of 6±0.7mm. The ZnO and c-zac showed promising antibacterial action against human bacterial pathogens, making them useful in the medical field. The synthesized materials have great activity on gram positive bacteria than gram negative bacteria. Thus, the c-zac heterostructure has a promising future outlook and scale-up potential as a catalytic and antimicrobial agent.

Keywords: *ZnO nanocomposite, solution combustion synthesis, doping, photocatalysis, antibacterial activity.*

1.INTRODUCTION

1.1 Background

With the rapid development of industrial society, increasing environmental safety threats pose the current global concern. Nowadays, water pollution is one of the most significant problems in the environmental field. The textile industry is one of the water-consuming and heavily polluting industries (Emmanuel, Adesibikan, and Saliu 2023). It is estimated that over 500 tons of various dyes are being discharged into the water bodies, and approximately 80% of them are from the textile industry. Since these dyes are poorly biodegradable and have many functional groups, they are potentially harmful to humans life and cause chronic effects (Areerob et al. 2018). Besides, according to the annual reduction in global gross domestic product prediction, by 2050, Asia and Africa will continue to share the highest-burden due to antimicrobial resistance, with 4.73 and 4.15 million deaths (Reali et al. 2019; World Bank Group 2017). Antibacterial materials have wide applications in combating bacteria (Raju et al. 2022).

Nanotechnology-based nanomaterials (NMs) and their synthesis have attracted the attention of researchers in the modern scientific world compared to that bulk materials (Khort et al. 2021; Saleh 2020). The semiconductor metal oxides are highly stable, non-toxic, inexpensive, and have superior catalytic properties among several nanomaterials. Zinc oxide (ZnO), a wide bandgap semiconductor (3.37 eV), has all the mentioned properties; however, it has limitations in antibacterial activity and ineffective degradation of pollutants under visible light irradiation (Ebrahimi et al. 2019). The antibacterial and photocatalytic properties of the materials are further enhanced by doping noble metal as an electron reservoir (Ciocci et al. 2023).

The unique properties of nanoscale materials (NMs), such as electronic density, charge distribution, and lattice distortion, greatly impact their applications (Roduner 2006). Effective doping of metal or metal ions, which creates either an n-type or p-type dopant, is one of the main ways to tune the magnetic, and optical properties. Besides, However, the dopant should substitute host atoms effectively so that decent dopant-host balance reactivity occurs. Selection of suitable host-dopant type, synthesis approach, solvent, and surfactant are the crucial parameters for balancing the reactivity. (Buonsanti et al. 2008; Jun, Choi, and Cheon 2006; Rahman, Balkhoyor, and Asiri 2019). The host-dopant type is essential for

the successful incorporation of the dopant in the host lattice. According to hard soft acid base (HSAB) theory, for the successful diffusion of the dopant ions into the host lattice, the hardness of the dopant should be less than that of the host in a hard base solvent like water (Gui et al. 2015; De Trizio and Manna 2016).

The properties of the doped materials are understood from advanced analytical techniques. The XRD pattern confirms the formation of local heterojunction and interstitial or/and substitutional incorporation depending on the angle shift. The optical properties of the doped materials are understood from DRS/UV-vis technique. Soft Lewis acid dopants (such as Ag and Cu) raise light absorption efficiency and also condense the bandgap by creating an inter band between the valance band (VB) and conduction band (CB) of the host (Agarwal et al. 2019). enhancing its application, especially in photocatalysis (Gunawan et al. 2012; Postica et al. 2019).

Several works have been conducted, and some are reported, for Ag- and Cu-doped ZnO NCs materials (Modwi et al. 2021a; Rakhsha et al. 2019; Xu, Chen, Hu, Liu, Q P Zhang, et al. 2020). Rakhsha et al. successfully synthesized the ZnO-based co-doped nanowire array materials using a chemical bath deposition approach; however, the application on the synthesized materials was not tested (Rakhsha et al. 2019). Xu et al. synthesized nearly spherical-shaped ZnO-based co-doped NCs using the one-step sol-gel method. The materials showed good methylene blue and methyl orange degradation properties (Xu, Chen, Hu, Liu, Q P Zhang, et al. 2020). Modwi et al. synthesized the same co-doped material based on the sol-gel method and got quasi-spherical shape morphology. In this study, the authors did not test the application of the materials (Modwi et al. 2021a). Most of the above-mentioned research works reported the parent/host materials properties improvement due to the copper and silver incorporation. However, none of these researches reported synthesizing porous materials based on the SCS approach, specifically by forming surfactant complex. Moreover, the results are also reported without discussing the basic science, which means LaMer's nanocrystal development model and HSAB host-dopant reactivity balance theory. Optimizing several parameters such as surfactant amount and type, and precursors percentages are crucial for catalyst surface area and porosity improvement Solution combustion synthesis (SCS) is an effortless, time-/energy-efficient method and creates regularly ordered porous materials.

Thus, this study aims to synthesize HSAB selected Cu- and Ag-doped and Cu and Ag co-doped ZnO nanocomposite materials using a time-/energy-efficient sol-gel combustion synthesis approach. Advanced analytical techniques will be used to understand the properties of the synthesized materials. The work also provides awareness about dopant-host reactivity balance, doped materials property, characterization techniques, and porous crystalline frameworks. Besides, the photocatalytic degradation of dyes and antibacterial activities of the synthesized materials will also be investigated.

1.2 Statement of problem

Controlling the adverse impacts of pollutants and improving the human living environment are so essential. Inorganic and organic dyes, as well as microbials, are among the contaminants found in wastewater. All of the toxins released into the environment by wastewater are hazardous to humans and the environment. As a result, pollutant removal has become critical(Shoran, Chaudhary, and Sharma 2022). There are many treatment methods for removal of pollutants such as bacteria and dye, for example bacterial infections were treated early by antibiotics but resistance of bacteria to commonly used antibiotics has made it more difficult for communities to choose an effective antibacterial treatment. Antibiotic-resistant bacteria, viruses, and other pathogens have made controlling many infectious diseases extremely challenging. At the same time, due to the increased prevalence of infectious diseases, people with antibiotic-resistant infections may be unable to get or afford any of the available treatments. To partially cover this gap, Nanomaterials (NMs) have lately been offered as a viable, cost-effective, and environmentally acceptable alternative to traditional treatment materials(Tang et al. 2022). Because of their nanoscopic/nanoscale size, NPs have the unique ability to cross the bacterial cell membrane and kill the bacterium. However, the efficiency of antibacterial NPs against pathogens of interest is mostly determined by their size and stability. To address the issue of stability, various researchers have added dopants or stabilizers to metal or metal oxide(Barui, Kotcherlakota, and Patra 2018).

Historically, dye removal was accomplished by a variety of methods, including biological, chemical, and physical methods. However, biological therapy is ineffective since colors are not biodegradable. As a result, biodegradation will take a long time to complete. Physical wastewater treatment methods entail physically capturing and removing contaminants from water. The treated water contained no dye, but because the process is non-destructive, the

contaminants remained and were not removed. This ultimately leads to cross-contamination, which is undesirable. On the other hand, chemical methods basically focus on the intuitive relationship between selected chemicals and toxic substances contaminated by chemical disinfection. (Khan et al. 2020). Photocatalytic degradation of organic dyes and pollutants is one of the most efficient and low-cost techniques to achieve this goal. Photocatalysis is a promising method for eliminating dangerous organic pollutants from industrial wastewater, and it has the potential to address some of the most serious environmental issues produced by contaminated water. Methylene blue can be degraded more effectively by photocatalysis, some of the photocatalysts utilized have downsides, such as recombination of photogenerated electrons and electron holes, which reduces the rate of degradation (Modwi et al. 2021b). This issue will expect to be solved by developing Ag and Cu co-doped ZnO nanocomposite materials via a sol-gel auto-combustion technique.

1.3 Objectives of the study

1.3.1 General Objective

The general objective of this study is to Synthesis of Cu-Doped ZnO/Ag/CuO Heterostructure for antibacterial and methylene blue dye degradation applications.

1.3.2 Specific objectives

- To synthesize ZnO NPs, Cu and Ag co-doped ZnO NCs and Cu-Doped ZnO/Ag/CuO Heterostructure using sol-gel solution combustion synthesis.
- Optimization of synthesis temperature and calcination time for ZnO nanoparticle.
- To characterize the synthesized NPs and NCs using different analytical techniques such as TGA, FTIR, PL, DRS-UV-vis, XRD, and SEM-EDX.
- To evaluate the antibacterial activities of as-synthesized NPs and NCs against gram-positive (*Staphylococcus aureus and Streptococcus Pyogenes*), and gram-negative (*Escherichia coli and Pseudomonas aeruginosa*) bacteria.
- To investigate the methylene blue degradation capabilities of synthesized NPs and NCs materials.

1.4 Significance of the study

Many antibacterial complexes and nanomaterials have lately been developed. Zinc, silver, and copper are important components for human and animal health in small levels, as well as have antibacterial activity. They can also be altered to be photocatalytic active materials, as a result, this study is designed to take on this challenge of evaluating the antibacterial and photocatalytic activity of silver and copper co-doped ZnO NP. The findings of this study may assist governmental and nonprofit groups in obtaining alternative antibacterial materials, and advanced method for dye treatment from waste water as well as the scientific community as an input in doing additional research on nanomaterials (Rabbani et al. 2021). It is also inevitable that industries are going to be benefited in their action to deal with their wastes.

1.5 Scope of the Study

The scope of this study was limited to the synthesis of ZnO and Cu and Ag co-doped ZnO using a simple and facile method; optimization of parameters for synthesis; characterization of synthesized nanoparticles and nanocomposite by using XRD, TGA, DRS, PL, FTIR, SEM-EDX, TEM, and UV-Vis spectroscopy; antibacterial tests of the synthesized nanoparticles and nanocomposite against antibiotic resistant bacterial strains such as *E. coli, P. aeruginosa, S. aureus, and S. pyogenes*. In addition, photocatalytic activity was also evaluated using methylene blue dye.

2. LITERATURE REVIEW

2.1 water pollution

Water pollution occurs when dangerous substances, most typically chemicals or microbes, pollute a stream, river, lake, ocean, aquifer, or other body of water, lowering water quality and making it poisonous to humans or the environment (Ahmed et al. 2018). Water contamination is a major problem that endangers human health. Every year, unsafe water kills more people than war and all other types of violence combined. Water is one of the most important natural resources for all living creatures to live in a sustainable and quality manner (Seidel et al. 2016). Because of the rapid increase of industrialization, urbanization, and population, global water consumption must climb above average. As a result, the world's scarcity of clean water sources is being exacerbated by an extremely pressing need for water. Water pollution has spiraled out of control, resulting in an increase in waterborne illnesses over the world. (Pandey et al. 2014).

Water-borne pathogen pollution in surface water bodies, as well as linked diseases, are serious water quality concerns around the world. Pathogen contamination is a severe issue for practically all forms of ambient water bodies, making its identification and comprehension critical(Pandey et al. 2014). Also, the extensive prevalence of organic dyes in industrial wastewaters from the paper, textile, and garment industries causes significant pollution of the environment. Rivers have been reported to be contaminated by partially treated or untreated discharges from chemical, petrochemical, and oil refineries, as well as oil spills, rolling steel mills, untreated residential sludge, and pesticide runoff (Rafiq et al. 2021). It should be noted that the comparatively high durability of synthetic dyes causes health and environmental problems due to their poisonous, mutagenic, and carcinogenic properties(Rafiq et al. 2021). Because of their aromatic chemical makeup, synthetic dyes are generally easy to detect but difficult to remove from wastewater and surface water habitats so researchers seek for treatment of pathogens and dyes by different techniques(Chahar et al. 2023; Sewnet et al. 2023).

2.2 Methods for water treatment

Water purification technology dates back to circa 1804 in Scotland, when the world's first citywide municipal water treatment plant was established utilizing sand filter technology. Humphrey Davy introduced the first method of disinfection in 1814, using chlorine, which was later applied to water disinfection about 1902(Ojha 2020). After a few years, ozonation

was introduced as a new method of water disinfection. Waterborne pathogen therapy has come a long way since then. Because of its ease of use and low cost, chlorination is still employed as a method of water disinfection. For the elimination of biological pollutants, numerous techniques have been proposed, including physical processes such as adsorption, heating (boiling), distillation, and filtration, biological processes in the form of activated sludge, chemical processes such as flocculation and chlorination, light irradiation, and photocatalysis(Piaskowski, Świderska-Dąbrowska, and Zarzycki 2018). The inefficiency of popular chemical disinfectants (chlorine, chloramines, ozone, chlorine dioxide, and so on) has driven the demand for more efficient pathogenic inactivation solutions. These traditional water disinfection treatments have been shown to be ineffective in the long run. A number of adverse effects and restrictions have been proposed for conventional pathogen inactivation approaches. Also, Adsorption, photo-oxidation, chemical oxidation, advanced oxidation processes (AOPs), biodegradation, filtering, coagulation, and other technologies have been developed to remove dyes in wastewater(Ojha 2020). These widely used methods, however, have limitations and disadvantages. Adsorption, for example, is a much-commended technique, but conventional adsorbents usually have drawbacks such as low adsorption capacity and kinetics, high regeneration cost, and column fouling; hence, new adsorbents are always needed(Cai et al. 2017). The AOPs have been widely researched and used to clean organic dye-contaminated wastewater. However, many photocatalysts' photocatalytic activity must still be improved, which is always accomplished by increasing visible light absorption, preventing excited electron-hole pair recombination, and increasing specific surface area (Binazadeh et al. 2023).

2.3 Nanotechnology

Nanotechnology is technology that is implemented at the nanoscale and has real-world applications (Malik, Muhammad, and Waheed 2023). Nanotechnology is a rapidly growing discipline with applications in science and technology for the purpose of creating new materials at the nano size level. Nanotechnology is concerned with the synthesis, characterization, and application of nanoparticles by manipulating their shape and size. Nanotechnology, also known as molecular system/device manufacturing, is a multidisciplinary scientific field that is rapidly evolving (Chahar et al. 2023). Nanomaterials' unique physical and chemical features can be used for societally beneficial purposes. Nanotechnology is a megatrend that has evolved into a general-purpose technology. Nanotechnology is no longer limited to research labs or small-scale manufacturing units of

nanomedicine, but has played a significant role in a variety of businesses. Companies all around the world are currently attempting to use nanotechnology to make their innovations more efficient in terms of structure, functioning, and designing view and productivity(Osherov et al. 2023). Nanotechnology has enabled the globalization of almost every industrial domain, from small-scale manufacturing and processing units in the agriculture, food, and medicine industries to larger-scale production units in the automobile, civil engineering, and environmental management industries. Nanotechnology has resulted in the global upgrading of practically every industrial domain(Salem 2023).

2.4 Synthesis of nanomaterials

As shown in Figure 2.1, nanoparticles can be manufactured utilizing a range of ways, including physical, chemical, and biological processes (Baig et al. 2021).

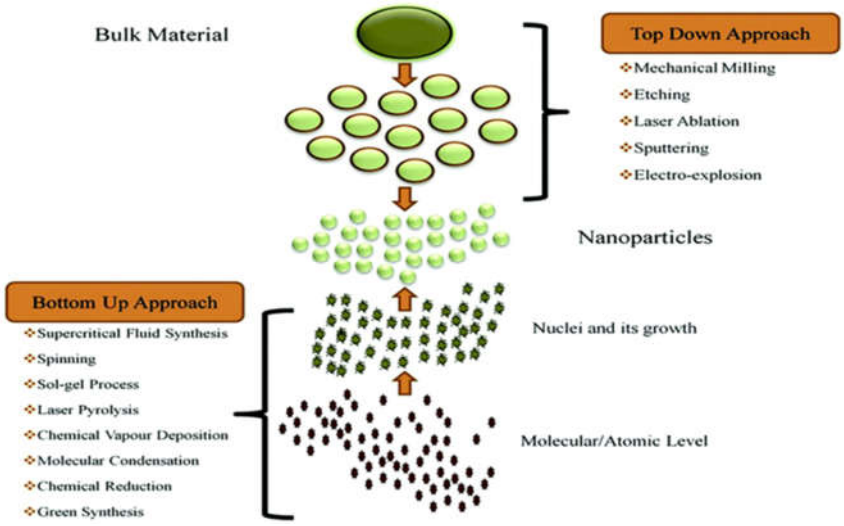

Figure 2. 1: Synthesis of nano material via top-down and bottom-up approaches (Baig et al. 2021).

2.4.1 Pre nucleation

Prenucleation: Occurring before nucleation; occurring before the formation of a nucleus(Gebauer and Cölfen 2011). Pre-nucleation clusters (PNCs) have proven important to understand the formation and growth of several materials, where different pre-nucleation clusters were stable in different solvents, and found to directly influence the final atomic structure (Ramamoorthy et al. 2020). Prenucleation clusters are solutes with “molecular” character in solution (Gebauer & Cölfen, 2011). The nucleation stage was discovered to be dependent on the size and reactivity of the PNCs. A schematic overview of possible nucleation and growth mechanisms are summarized in Fig. 2.2. Cluster is considered as

building units for the nanocrystals. Nucleation is the very first stage of the formation of a new phase for any crystallization process and is critical step for the following growth process and the resulting morphology of the nanocrystals (Bakken, Grendal, and Einarsrud 2023).

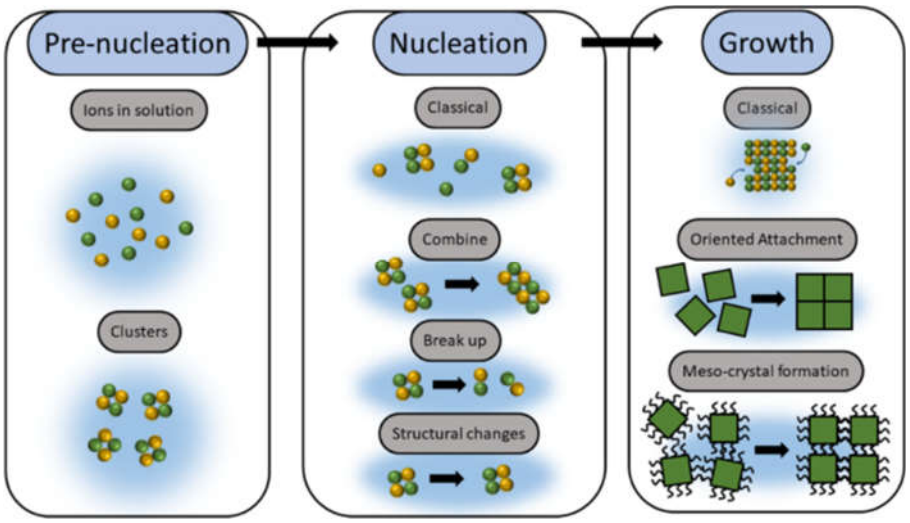

Figure 2. 2: Schematic diagram of stepwise formation of clusters up to growth (Bakken et al. 2023).

2.4.2 Nucleation and growth of nanomaterials

Controlling the nucleation and growth development processes preceding the creation of nanocrystals is critical(Tang et al. 2020). LaMer's group theory was the first model to explain precursor decomposition and reduction, nucleation, development into seeds, and finally growth into nanocrystals in solution. The process of forming a new thermodynamic phase from an old phase with a high free energy to an organized structure or pattern with a low free energy is known as nucleation. Classical nucleation theory (CNT) is based on the concept of critical nuclei, which act as transition states between supersaturated solutions and growing particles. Their surplus standard free energy is affected by supersaturation and determines the height of the phase separation barrier. According to the LaMer model, the whole nucleation and growth process can be divided into three phases (see Fig. 2.3)(Schladt et al. 2011) . In the first phase, the monomer concentration increases gradually until it reaches the point of supersaturation (S). If no seeds (like dust particles or small crystallites) are present, which would initiate heterogeneous nucleation, only homogeneous nucleation is possible. However, since the energy barrier for the initiation of a homogeneous nucleation event is considerably high, the monomer concentration can further increase (phase II). In phase II, the supersaturation finally reaches a critical value (Sc), which means that the system contains enough energy to overcome the energy barrier(Laganà et al. 2023). Therefore,

homogeneous nucleation throughout the entire reaction solution can take place any time. Eventually, a large number of nuclei are formed simultaneously in a process that can best be described as a nucleation “burst”. As a consequence, the monomer concentration drops drastically below a point where no further nucleation is possible. Finally, in phase III, all nuclei grow at the same time, and, since their growth histories are identical, the NPs will end up having an exceptionally narrow size distribution (Soltani et al. 2012)

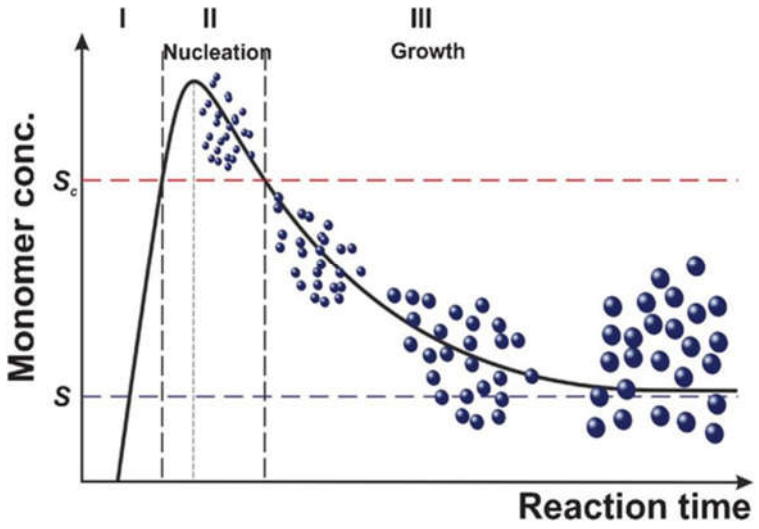

Figure 2. 3: LaMer model, the whole nucleation and growth process (Schladt et al. 2011).

2.5 Difficulties during synthesis method and parameter optimization.

Several parameters, including the synthesis technique, pH, temperature, pressure, time, particle size, pore size, the method of treating aggregation, nucleation, and nanoparticle growth, have a significant impact on the quality and quantity of generated nanoparticles, as well as their characterization and uses (Hachem et al. 2022).

2.5.1 Aggregation

Aggregation is a thermodynamic process that causes problems when certain conditions are satisfied. Temperature; the concentration, content, and surface charge of the nanoparticles; the dielectric constant and ionic strength of the medium; the presence of surfactants, solution pH, dissolved ions, naturally occurring organic matter, clays, and bio colloids are all factors(Johnson et al. 2021). Because aggregation is irreversible, all of these characteristics must be regulated from synthesis to final nanoparticle application to achieve adequate material and process control (Shrestha, Wang, and Dutta 2020). In comparison to the bulk material, a bigger function of the atoms is at the surface, promoting various interactions with its surroundings. Furthermore, the reduction in size affects the material's electrical structure,

resulting in unexpected quantum effects. Size also has an impact on mobility, which is predominantly governed by Brownian motion for NPs and is important in biological and environmental processes. The small size, however, results in a high surface energy, and NPs tend to combine, lowering the surface energy. Uncontrolled NP aggregation can have detrimental consequences in all applications and should be avoided. There are, however, examples of controlled NP aggregation that results in unique effects (Aravind, Amalanathan, and Mary 2021; Johnson et al. 2021).

2.5.2 Calcination temperature

Calcination is the process of heating a material to a specific temperature and in a specific atmosphere. The particles fuse and enlarge the primary crystallite size during the calcination process. This is known as particle coarsening, a phenomenon that occurs in solid (or liquid) solutions and is frequently employed to produce larger crystals from smaller crystals, resulting in a reduction in the number of smaller particles while larger particles continue to grow. With increasing calcination temperature, the pore volume decreases, leading to compact shrinkage(Li and Kaner 2006). As Dutta reported, with the increase in the calcination temperature from 400°C to 600°C, the specific surface area of ZnO nanoparticles significantly decreased from 22.9 to 2.6 m^2(Dutta, Paul, and Chattopadhyay 2016).

2.6 Nanoparticles and their application

A nanoparticle, also known as an ultrafine particle, is a matter particle with a dimension of 1 to 100 nanometers (nm). Nanoparticles cannot be observed with standard optical microscopes, necessitating the use of electron microscopes or laser microscopes. Dispersions of nanoparticles in transparent fluid can also be transparent for the same reason (Pandit et al. 2022). Nanoparticles have a unique size-dependent feature known as high 'aspect ratio,' which is the surface area to volume ratio. The aspect ratio increases as particle size decreases. In other words, they have a larger surface area than volume. The increased surface area of the smaller nanoparticles increases their reactivity with the surrounding molecules (Zeng et al. 2023). Antibacterial characteristics are possessed by nanoparticles (NPs). Because of their propensity to produce reactive oxygen species (ROS), nanoparticles have a great potential as antibacterial agents. The creation of reactive oxygen species impairs the antioxidant defense system, reduces Adenosine triphosphate (ATP) synthesis, and causes mechanical damage to the cell membrane. Recent research has revealed that the modification has a significant impact on ROS formation by introducing different dopant elements into them (Espitia et al. 2012). Positively charged nanoparticles were found to be capable of

altering the operation of the electron transport chain in bacteria. It has previously been hypothesized that the formation of hydrogen peroxide from the surface of zinc oxide is an effective means for bacterial growth inhibition. These improved antibacterial drugs attack germs locally while being non-toxic to surrounding tissue. Nanoparticles anti-bacterial mechanism is described in Figure 2.4 (Ijaz et al. 2020).

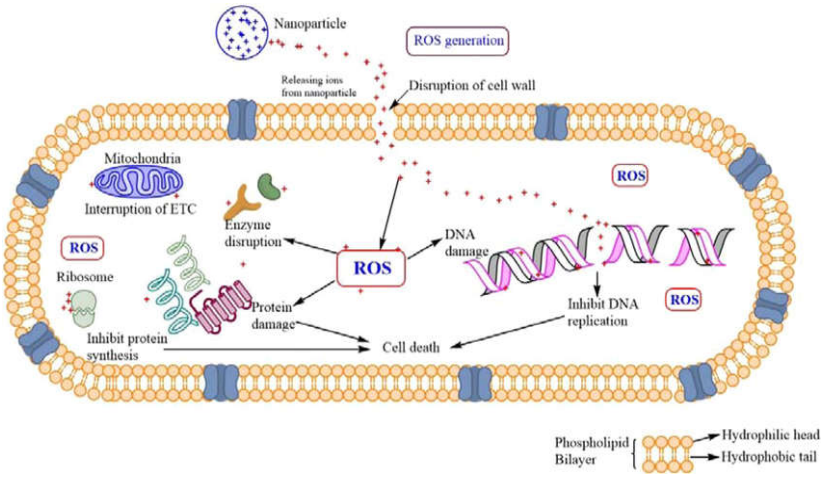

Figure 2. 4: Overall antibacterial mechanism of nanomaterials (Ijaz et al. 2020).

2.6.1 Zinc oxide nanoparticle

ZnO is a polar II-VI compound semiconductor with ionicity that falls somewhere between covalent and ionic semiconductors (Ong, Ng, and Mohammad 2018). Because of the divergence from stoichiometry and the presence of intrinsic defects such as O vacancies (VO) and Zn interstitials (Zni), it is an n-type semiconductor. ZnO is a semiconductor with a large exciton binding energy of 60 meV and a wide band gap of 3.37 eV. ZnO is a good replacement to TiO_2 in terms of band energy. It is also an environmentally acceptable substance that does not produce hazardous byproducts (Rajeshkumar, Lakshmi, and Naik 2019). ZnO offers a number of attractive features, including non-toxicity, biocompatibility, high stability, outstanding transparency, strong room-temperature luminescence, high electron mobility, and high photocatalytic activity. Solar cells, laser diodes, thin-film transistors, UV lasers, optoelectronics, gas sensors, transparent conductive contacts, light emitter diodes, surface acoustic wave devices, and piezoelectric devices all use ZnO nanoparticles in some way. ZnO nanoparticles have been employed in a variety of applications, such as electronics, optics, cosmetics, and photocatalytic destruction of organic contaminants in water(Rabbani et al. 2021). When compared to other metal oxides, ZnO has a high degree of lattice defects on its surface area, making it an efficient photocatalyst

material. Phase purity, crystallite size, surface area, dopant type, and synthesis procedures are all key factors in determining ZnO NP photocatalytic activity Figure 2.5 summarize application of ZnO nanoparticle (Kołodziejczak-Radzimska and Jesionowski 2014).

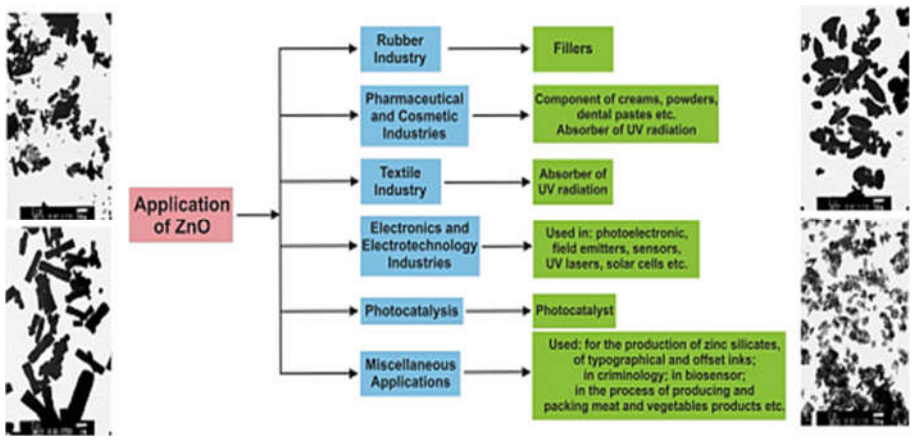

Figure 2. 5: Application of ZnO nanoparticle (Kołodziejczak-Radzimska and Jesionowski 2014).

2.6.1.1 Application of ZnO nanoparticle as anti-bacteria

In recent decades, ZnO nanostructures have proven to be more hazardous to bacteria and less sensitive to human cells when compared to other metal oxides with anti-bacterial capabilities. ZnO nanostructures' antibacterial mechanism described in Figure 2.6 comprises the generation of reactive oxygen species (ROS) such as hydrogen peroxide (H_2O_2), hydroxide ion (OH^-), and peroxide ion (O_2^{-2}). ROS is a significant toxicity mechanism that includes cell wall breakdown due to the interaction with ZnO nanostructures(Chauhan et al. 2020). Because of surface defects and ROS production in the dark, ZnO nanostructures can have higher antibacterial activity. When ZnO nanostructures interact with bacterial cells, they produce mitochondrial weakening, intracellular outfow, and oxidative stress, which finally slows bacterial development and destroys the entire cell(Qi et al. 2017).

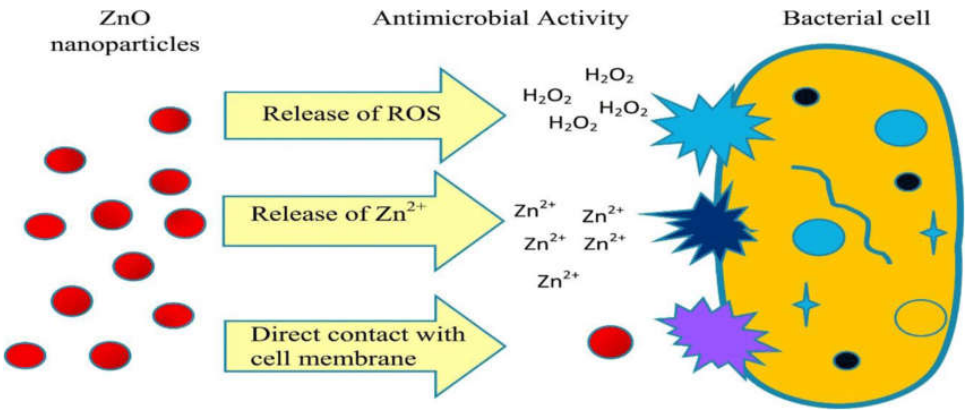

Figure 2. 6: Basic mechanism of anti-bacterial activity of ZnO nanostructures (Chauhan et al. 2020).

2.6.1.2 Application of ZnO nanoparticle for photocatalysis

ZnO is a very promising photocatalyst for photocatalytic elimination of water contaminants such as phenol and its derivatives when exposed to UV or sunshine. It provides various benefits, including: (i) quick degradation rate, (ii) mineralization of organic compounds to green products, (iii) capacity to work at ambient temperature and pressure, and (iv) reduction in organic compound toxicity(Ong, Ng, and Mohammad 2018). Figure 2.7 describes photocatalysis mechanism of ZnO nanoparticle. This technique produces highly potent chemical oxidants in situ using ozone (O_3), hydrogen peroxide (H_2O_2), Fenton's reagent, UV light, or a catalyst. The hydroxyl radicals ($OH^{\cdot}$) produced are powerful oxidants capable of oxidizing refractory organic molecules (Alshehri and Malik 2019).

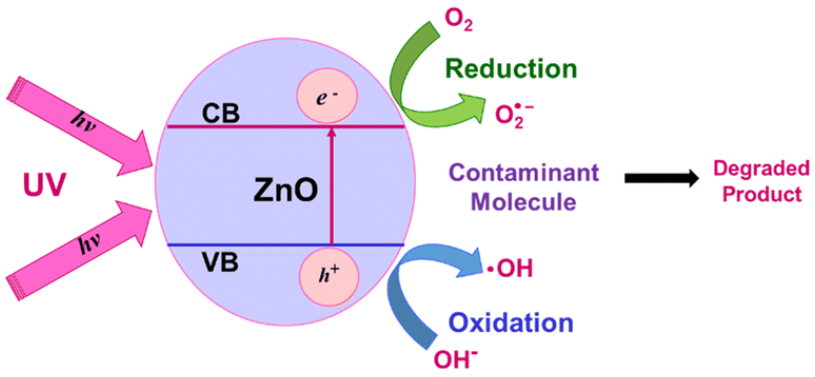

Figure 2. 7: ZnO nanoparticles exhibited excellent photocatalytic activity (Alshehri and Malik 2019).

2.6.1.3 Improvement of ZnO as photocatalysis

Low quantum yield and a high photogenerated electron-hole pair recombination rate limit ZnO's photocatalytic activity. Because of this recombination process, the quantum yield is decreased and energy is lost. The electron-hole recombination route should be minimized to allow for efficient photocatalysis. The recombination problem may be resolved by metal and non-metal doping by enlarging the charge gap between electrons and holes(Chauhan et al. 2020). Additionally, dopants might capture electrons, reducing the likelihood of electron-hole recombination, which would render the photocatalytic system inactive. Doping accelerated the photocatalytic degradation of dyes, with doped-ZnO degrading pollutants faster than undoped ZnO due to changes in bandgap energy and surface area. A larger surface area indicates a strong redox reaction; it produces more electrons and holes, boosting the band gap; the particle size reduces, which energetically participates in or correlates with the photocatalytic reaction; and the whole process has a higher degradation rate. As a result, doping is a straightforward and effective procedure(Lee and Jun 2019).

2.7 Doping of semiconductors

Doping is the process of combining a semiconductor with a certain impurity in a controlled amount. p-type and n-type doping are the two types of doping(Al-Zaqri et al. 2022). Doping has an important role in determining the physical properties and uses of numerous materials, particularly semiconductors(Rabbani et al. 2021). This idea has been validated by extremely successful implementations in the semiconductor sector. Minor contaminants influence the carrier concentrations and electrical conductivities of materials. Fundamentally, a good dopant should be highly soluble in its host material and have a low defect level(Neto et al. 2019).

Doping will cause various changes to the electronic band structure of semiconductors (Fig. 2.8), such as (i) the formation of intra band energy states, (ii) the narrowing of the bandgap, and (iii) the formation of impurity bands in degenerately doped transition metal semiconductors, which will broaden the absorption range of the materials to some extent. In the first example, doping generates local states that serve as dominant centers for optical excitation and relaxation, extending the absorption tail of the absorption curve to longer wavelengths (Fig. 2.8b) when compared to an intrinsic semiconductor (Fig. 2.8a). The second impact of doping is a change in the position of the conduction or valence band, which results in a constriction of the bandgap (Fig. 2.8c) and hence a red shift at the absorption spectrum's edge. This strategy for expanding a solar absorber material's light absorption has

been shown in solar steam generating applications (Fig. 2.8d). Furthermore, doping not only broadens the optical absorption spectrum but also increases photothermal conversion efficiency due to the increased likelihood of nonradiative recombination in the presence of additional free carriers in the semiconductor(Ong et al. 2018).

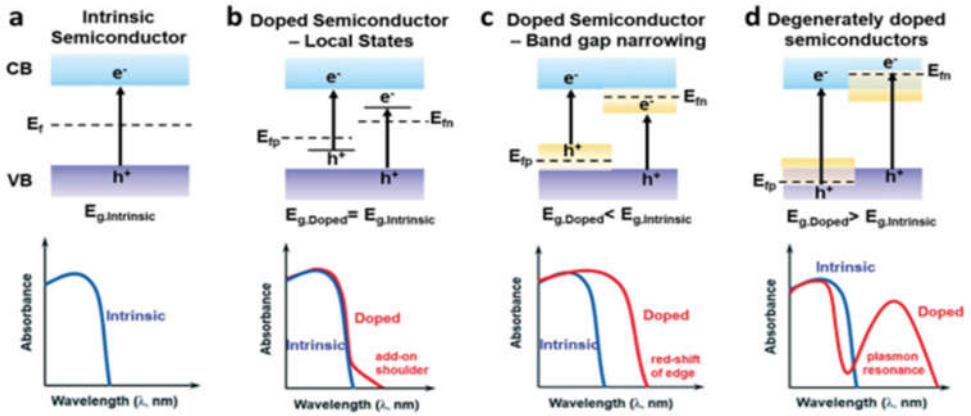

Figure 2. 8: Schematic for bandgap engineering of semiconductors (Ong et al. 2018).

2.7.1 Copper doped ZnO

The most effective way to raise ZnO's photocatalytic performance is by using Cu. The electrical, optical, and magnetic characteristics of ZnO are substantially altered by Cu doping. By causing lattice defects in ZnO due to Cu doping, optical absorption in the visible region is increased, which improves photocatalytic activity(Bukhari et al. 2021). There have been some published investigations on Cu-doped ZnO nanostructures. Cu-ZnO NPs were synthesized by Min et al. (2011) using a sol -gel technique and their optical and photocatalytic characteristics were examined (Ijaz et al. 2020). Kurioskar et al created Cu-ZnO NPs using a straightforward chemical process, and their structural, optical, and photocatalytic behavior was investigated (Kuriakose et al., 2015). By using a simple wet chemical process, (Ijaz et al. 2020) created Cu-ZnO nanostructures and discovered that they had higher photocatalytic activity than ZnO that had not been doped(Raju et al. 2022)

2.7.2 Silver doped ZnO

Ag-doped ZnO catalyst is employed in a variety of applications, including phenyl hydrazine chemical sensor applications, anti-bacterial activity, and photocatalytic degradation of many types of dyes in water(Bechambi et al. 2015). Ag in ZnO minimizes the recombination of electron-hole pairs. In aqueous solution, zinc oxide releases Zn^{2+} ions, whereas silver releases (Ag^{+}) ions, both of which contribute to antibacterial efficacy. The released Zn^{2+} and Ag^{+} ions significantly contributed to nanoparticles' overall antibacterial effect and

photocatalytic activity(Alqadi et al. 2022). Figure 2.9 shows the photocatalytic degradation mechanism of MB dye by Ag-doped ZnO(Alqadi et al. 2022).

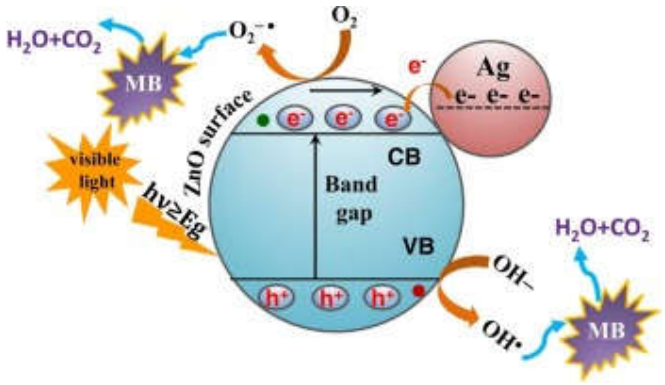

Figure 2. 9: Photocatalytic mechanism of Ag doped ZnO (Alqadi et al. 2022).

2.7.3 Co-doping of semiconductors

Simultaneous doping of two kinds of atoms (co-doping) into semiconductor materials has recently been realized and it may result in higher photocatalytic activity and special characteristics compared with single element doping into semiconductor oxides(Kulyk et al. 2009; Zno et al. n.d.). In the case of wide band-gap materials, the problems are severe. For example, n-type doping was found to be difficult for high conduction-band minimum (CBM) energy; on the other hand, p-type doping was found to be difficult for low valence-band maximum (VBM) energy, as a result, bipolar doping problems exist in many wide band-gap semiconductors, where either n-type or p-type dopants can be doped, but not both, therefore, a feasible solution is to simultaneously incorporate certain amounts of p-type and n-type dopants, for lowering their formation energy, which is also the fundamental principle of compensated co-doping(Kulyk et al. 2009). Co-doping has been proposed as a solution to the problems of bipolar doping and compensation in semiconductors. In general, co-doping can be efficient for increasing dopant solubility, increasing activation rate by lowering the ionization energy of acceptors and donors, and increasing carrier mobility(GuruSampath Kumar et al. 2020).

2.7.4 Ag-Cu doped ZnO

Doping a ZnO photocatalyst with transition metal or noble metal ions may result in crystal defects and alter the optical characteristics of ZnO, hence boosting the photocatalytic activity of produced nanoparticles (NPs)(Copaciu et al. 2012). Under sunlight, valence band electrons in these NPs can be stimulated to the conduction band while simultaneously forming an equal number of holes in the valence band by photons with energies larger than

or equal to ZnO band gap electrons(Aravind et al. 2021). Electrons can flow from ZnO to Ag+/Cu NPs because the conduction band energy level of ZnO NPs is higher than that of the intra band state of Ag-doped ZnO and Cu-doped ZnO NPs. As a result, oxygen vacancy defects and Ag/Cu on the surface of ZnO NPs capture electrons and prevent e-h+ pair recombination. Noble metal deposits on the ZnO surface effectively separate electron hole pairs by attracting conduction band electrons(Chauhan et al. 2020). When UV light strikes ZnO, electrons in the valence band (VB) are transported to the conduction band (CB), resulting in the production of the same number of holes in the VB(Alqadi et al. 2022). The photogenerated electrons from the semiconductor can be trapped by Ag or Cu on ZnO, which operate as electron sinks. As a result, photogenerated charge carriers can be efficiently segregated, improving the photocatalytic activity of Cu or Ag-doped ZnO under UV irradiation. Figure 2.10 shows the overall mechanism of photocatalytic activity of Ag-Cu doped ZnO nanoparticle(Xu, Chen, Hu, Liu, Q. P. Zhang, et al. 2020).

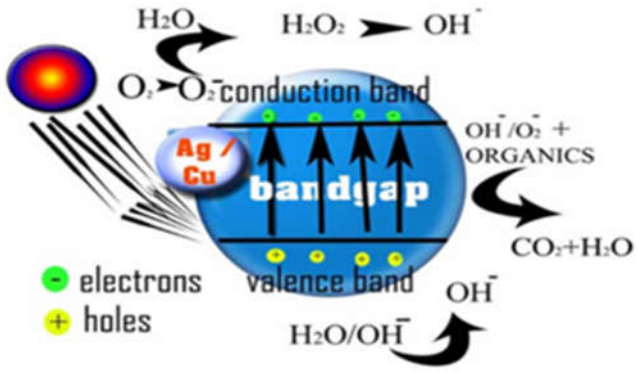

Figure 2. 10: Mechanism of photocatalytic activity of Ag-Cu doped ZnO (Xu, Chen, Hu, Liu, Q. P. Zhang, et al. 2020).

In addition to photocatalysis numerous studies have proven that Ag-Cu doped ZnO modification is one of the most efficient ways for increasing the antibacterial activity of ZnO nanoparticles(Alqadi et al. 2022; Osherov et al. 2023; Raju et al. 2022).

3. MATERIALS AND METHODS

3.1. Description of the Study Area

The study was carried out in Adama Science and Technology University, Applied Chemistry, Applied physics, and Materials Science and Engineering Laboratories. and chemicals were purchased from authenticated chemical markets. The material synthesis was carried out entirely at Adama Science and Technology University (ASTU) in applied chemistry laboratory. Photocatalytic activity, XRD, and UV-vis spectroscopy analysis was performed in ASTU material science and engineering laboratory. PL was performed in Applied physics laboratory. FTIR was performed in Bahir-dar university, UV-vis- DRS, TEM, and FESEM-EDX analysis was performed in India.

3.2. Chemicals and Reagents

The chemicals and reagents were analytical grade and used without further purification. Zinc nitrate hexahydrate (Zn $(NO_3)_2$. $6H_2O$ (Sigma Aldrich, 99%, Germany), Copper nitrate trihydrate (Cu $(NO_3)_2$. $3H_2O$ (Sigma Aldrich, 99%), silver nitrate hexahydrate (Ag $(NO_3)_3$. $6H_2O$ (Sigma Aldrich, 98%), Poly (vinyl alcohol) (PVA, Thermo Fisher Scientific India Pvt. Ltd.), methylene blue ($C_{16}H_{18}C_lN_3S$) (Sigma Aldrich) Muller Hinton agar and distilled water, were used throughout the experiment.

3.3 Synthesis of Nanomaterials

3.3.1 Synthesis of ZnO NPs

The ZnO NPs were synthesized by the sol-gel solution combustion synthesis as reported in previous work (Aravind et al. 2021) with slight modifications such as adding surfactant as a stabilizing agent. In detail, first, the surfactant polymer was dissolved in the measured amount of distilled/deionized water at about 70 °C with stirring on a hot plate with magnetic stirrer (Jiamprasertboon et al. 2023). Then, an appropriate amount of the zinc salt precursor was added to the dissolved surfactant polymer solution at about 50 °C with stirring on a hot plate with magnetic stirrer. The mixture was further heated to the ignition temperature, the temperature at which combustion/self-propagation starts in the oven at temperature range of 150–210 °C. Finally, the formed solid was calcined at a TGA/DTA optimized temperature in the furnace to decompose the surfactant and oxidants.

Optimization of synthesis temperature and calcination time was also performed by varying the synthesis temperature from 30 °C to 90 °C while increasing the calcination time from 30 to 180 min at a fixed temperature of 450 °C.

3.3.2. Synthesis of Cu-doped ZnO/Ag/CuO Heterostructure

The Cu and Ag co-doped ZnO were also synthesized by dissolving 1 g of the PVA polymer in 50 mL of distilled water while stirring with a magnetic stirrer at about 70 °C for nearly 15 min. After that in this cooled PVA solution 1%, 5%, 10%, and 15% of Ag and Cu nitrate salts with 99%, 95%, 90%, and 85% of zinc nitrate salt, 0.25 molar concentration of each, was mixed in different beakers for just over half an hour of stirring to form solution. Each solution was then heated until a gel is formed. The gel produced at the stage of water dehydration, at about 70 °C, was further heated to the polymer–surfactant ignition temperature range of 150–210 °C (the temperature at which combustion and self-propagation began). Finally, the combusted material was crushed to reduce its size, calcined at 450 °C for 1 hour, and then used for further characterization and application.

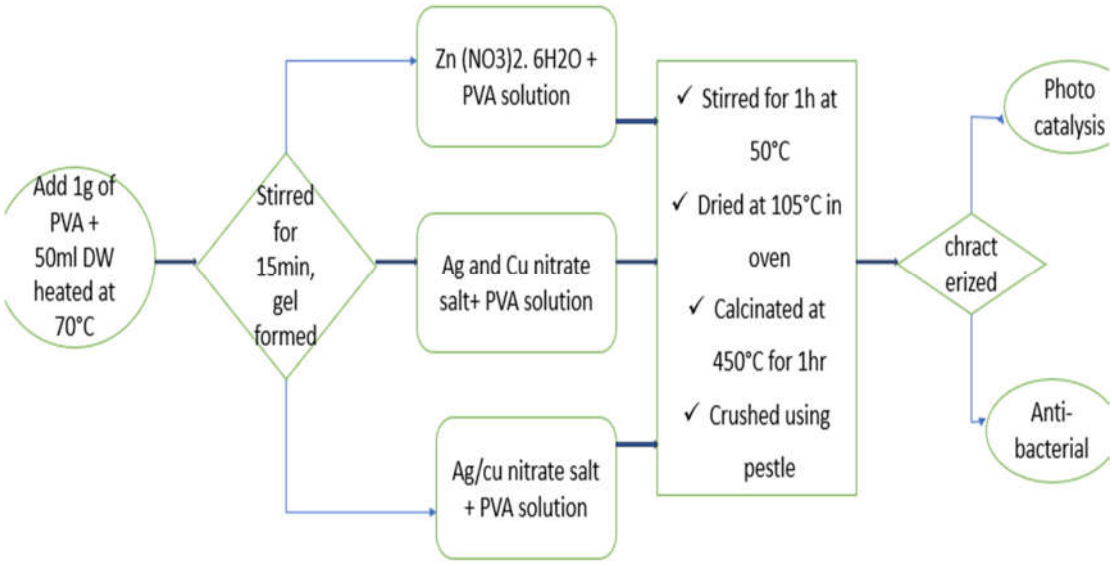

Figure 3. 1: Flow chart for the experimental procedures of the study.

3.4 Characterization

The synthesized ZnO NP, and Cu-doped ZnO/Ag/CuO Heterostructure, were subjected to characterization for the determination of temperature stability, crystalline or amorphous natures, optical properties, identification of functional groups and evaluation of size and morphology.

3.4.1. Thermo Gravimetric Analysis (TGA)

To estimate the calcination temperature of the produced material, TGA was performed using simultaneous DTA-TG equipment (DTG-60H, Shimadzu Co., Japan). In a platinum crucible

on the pan of the microbalance, 7.53 mg of uncalcined samples (ZnO nanoparticle) was heated from 23.30°C to 801.65°C, using Al_2O_3 as an inert material, at a heating rate of 20 degree/min(Guo and Peng 2015).

3.4.2.X-Ray Diffraction (XRD) analysis

To analyze and estimate the crystalline size of the synthesized nanoparticles, an X-ray diffractometer (DW-XRD-Y7000, DRAWELL, China) was used. The XRD data was recorded in terms of diffraction intensity versus 2θ from 10° to 80° and the result was plotted using Origin Pro software. The diffraction pattern also provided the information on size and shape of the unit cell from peak positions and information on electron density inside the unit cell. Also, the crystallite size was estimated using the Scherrer's formula (Kawsar et al. 2024).

From XRD data the crystallite sizes were determined by Scherrer's' equation (Eqn 1),

$$D = \frac{k\lambda}{\beta cos\theta} \qquad (1)$$

Where k is constant (which is 0.9 for spherical symmetry), λ is the x-ray radiation wavelength (which is 0.15406 nm), β is equal to the full width at half the maximum of the peak, and θ is the Bragg x-ray diffraction angle between the incident rays and the diffracting planes.

3.4.3. Photo Luminescence (PL) analysis

The emission of light from the synthesized nanoparticles was measured under optical excitation by using a photoluminescence instrument (S/N: MY18490002, Agilent Technologies, USA). For this analysis, about 5 mg of calcined ZnO nanoparticles and c-zac nanocomposites were suspended in DMSO in separate vials and sonicated for 30 min at 75 kHz by an ultrasonic bath(Yuan et al. 2020). The prepared nanoparticle suspension was added to the cuvette and subjected to PL scanning and data was recorded. The obtained data were plotted and analyzed as graphs by using Origin Pro (8.5 version) software.

3.4.4. UV-vis Diffuse Reflectance Spectroscopy (DRS) analysis

The optical properties of the synthesized Nanoparticles and nanocomposites were analyzed by using UV-vis spectrophotometer (Carry 100 UV-Vis, Agilent Technologies, USA). Samples are typically prepared as solid powders or films. It must be finely ground or dispersed to ensure uniformity and maximize light diffusion and mixed well with Barium

Sulphate. The prepared sample is placed in the sample holder of the DRS instrument and the reflectance spectrum is measured over the desired wavelength range, typically from UV to Vis. The band gap energy for ZnO nanoparticle, and c-zac nanocomposite, were calculated by using Kubelka-Munk function plots.

3.4.5. Fourier Transform Infrared Spectroscopy (FTIR) analysis

Fourier Transform Infrared Spectroscope (FTIR) (FT/IR-6600typeA, JASCO, Japan) was used to detect the changes of major functional groups residual of synthesized nanoparticle samples. For this purpose, a 0.5g synthesized nanoparticles powder were mixed along with IR-grade powder (KBr) and then this powder has been transferred into a sample cup of attenuated reflectance accessory and scanned in the spectrum region (4000 to 400 cm^{-1}). The FTIR spectral data were recorded and analyzed by using Origin Pro (8.5 version) software.

3.4.6. Field Emission Scanning Electron Microscope (FE-SEM) analysis And Energy Dispersive X-ray (EDX) spectroscopy analysis

Scanning electron microscope (FE-SEM, ZEISS SIGMA VP, Germany) is used to estimate the topography, morphology, and crystallographic information of synthesized nanoparticles and it was conducted for morphological analysis of the synthesized nanoparticles(Pham 2020). The nanomaterials were kept on a sample stub with carbon tape and the stubs were placed in the electron microscope sample chamber. The SEM analyses of the synthesized nanoparticles were recorded at different magnifications (2.5, 5, 10, 20, and 30 KX).

Energy-dispersive X-ray spectroscopy (EDX) (associated with SEM) was used to determine the chemical composition of the produced nanoparticles and nanocomposites. Energy dispersive X-ray spectroscopy (EDX) is an analytical technique used to determine the elemental analysis or chemical characterization of a sample via interaction between the sample and the X-ray excitation source (Sarmah and Kumar 2024). Every atom has a distinct arrangement of electrons in discrete energy levels around the nucleus while at rest. When a high-energy beam of radiation strikes a sample (matter), it may excite an electron from the inner shell, causing a hole to form. To compensate for this vacancy, electrons from the outer shell migrate to the inner shell, and the energy differential between the outer and inner shells can be generated in the form of an X-ray. Because each element has a distinct electronic configuration, when the sample is exposed to high-energy electromagnetic radiation, it emits a distinctive X-ray that acts as a fingerprint for each element. A detector can detect the number and energy of X-rays emitted by a sample.

3.4.7 Transmission electron microscopy, (TEM-HRTEM-SAED) analysis

For the determination of particle size, morphology, and crystallinity of nanoscale-sized materials(Li et al. 2020), further analysis of morphology by transmission electron microscopy, high-resolution transmission electron microscopy, and selected area electron diffraction analysis were performed using (JEOL JEM 2100 HRTEM, JEOL, USA).

3.5 Anti-bacterial Activity

3.5.1. Test strain collection

A total of four types of bacterial species were subjected to antibiotic assay. These are *S. aureus* (ATCC 25923) (Gram-positive), *P. aeruginosa* (ATCC 27823) (Gam-negative), *S. pyogenes* (ATCC 11778) (Gram-positive), *E. coli* (ATCC 25922) (Gram-negative) and all these strains were obtained from the Oromia regional laboratory, Adama. The bacterial strains were maintained in Muller Hinton Broth (MHB) (pH 7.2) at 37℃, and the stock culture slants were maintained in the refrigerator until use.

3.5.2. Standardization of inoculum

The active culture bacteria for the test were prepared by taking a loop full of bacterial cells from stock cultures and streaking them on Mueller Hinton Agar, and it was incubated at 37℃ for 24 hrs. The cell suspension of the above four bacteria was freshly prepared by transferring the isolated colony, which is 24 hrs old, into a test tube containing 10 mL of MHB and incubating it overnight. Then, fresh cultures were diluted by adding sterile saline solution and vortexed thoroughly. The turbidity of the suspension was matched with that of 0.5 McFarland standards, equivalent to 1.5×10^8 (Colony Forming Unit) CFU/mL for the sensitivity test as described by National Committee for Clinical Laboratory Standards (NCCLS) (Sharma et al. 2016).

3.5.3. Disk Diffusion Method

The In vitro, disc diffusion method was conducted to evaluate the antimicrobial activities of a synthesized ZnO NPs and c-zac Heterostructure (Communication and Detection 2016). The antibacterial activities were determined against four pathogenic bacteria. For this experiment, Muller-Hinton agar (MHA) media were prepared and autoclaved at 121℃ and 15 psi for 15 minutes. After autoclaving, media was poured into sterile petri plates up to a uniform thickness of approximately 4 mm and allowed to solidify. As mentioned above, the microbial inoculum was sub cultured into the MHB and incubated overnight for fresh

culture. Then, these inoculums were diluted to adjust with 0.5 McFarland standard. A sterile cotton swab was inserted into the culture suspension. The swab was then streaked on the surface of the Muller-Hinton. The swab was streaked three times over the entire plate surface to ensure a uniform, confluent growth. A 70 mg/mL of stock solution of each synthesized ZnO NPs and c-zac NCs were prepared by dissolving 70 mg in 1 mL of 10% DMSO. Each sample was formed for disc diffusion assay by serial dilution (70mg/mL, 60 mg/mL, 50 mg/mL, and 40mg/mL). A sterilized filter paper (Whatman No. 1, diameter = 6 mm) disc was dipped in the samples. Then, the samples were left to diffuse in the disc for 30 min and placed on the inoculated agar (KESKİN and ÖKSÜZ 2024). Sterilized paper disc soaked in 10 µg/Ml ciprofloxacin standardized antibiotic was used as a positive control. At the same time, a disc impregnated with DMSO was used as a negative control. The plates were incubated overnight at 37°C for 24 hr. Finally, the microbes' inhibition zone by antimicrobial agents was measured using ruler in mm scale.

3.6 Photocatalysis: methylene blue degradation

According to the method reported with modification (Rafiq et al. 2021) , the degradation of MB dye was used to test the photocatalytic activities of the synthesized samples(Chauhan et al. 2020). All of the tests were conducted in an open environment at ambient temperature. To verify the catalyst pollutant adsorption-desorption equilibrium in each experiment, 20 mg of metal oxide catalyst was introduced to 100 mL of MB solution (10 mg/L), followed by stirring for 30 minutes in the dark. The mixture was consistently mixed during the tests. The light was turned on, and a 150 W halogen lamp was used as the visible light source after 30 minutes of stirring in the dark. To separate the photocatalyst particles, 8 mL of the slurry was taken at predefined irradiation periods and centrifuged (3000 rpm, 20 min). The degradation efficiency in % was computed using Equation 2, and the MB concentration was determined using a UV-visible spectrophotometer (UV-3600Plus series) measuring the absorption maximum at λ max = 664 nm. In order to examine reaction dynamics, the pseudo-first-order kinetics equation (Equation 3) was used.

$$\text{Degradation yield (\%)} = \frac{C0-Ct}{C0} * 100 \qquad (2)$$

Pseudo 1st order and second order kinetics equation were utilized in the equations to determine the kinetics of photodegradation.

$$Pseudo-first-order\ kinetics;\ ln\frac{Ct}{C0} = -kt \quad (3)$$

$$Pseudo-second-order\ kinetics;\frac{1}{Ct}-\frac{1}{C0}=kt$$

Where C_0 is initial dye concentration (mg L^-), Ct is the dye concentration (mg L^-) at a time t and k is pseudo-first-order reaction rate constant (min^{-1})(Abebe, Zereffa, and Murthy 2021).

In this paper we use Pseudo-first-order kinetics because it simplifies the mathematical treatment of reactions. This simplification facilitates data analysis and allows determination of reaction rate constants. Additionally, this is preferred for the following reasons: In photocatalysis, the decomposition of dye molecules typically involves several steps such as Absorption of light, electron transfer, and generation of reactive species. The rate-limiting step that determines the overall rate of degradation is often the interaction of the dye molecules with the reactive species produced by the photocatalyst. Assuming that this step is much slower than the other steps, the entire reaction can be approximated as a pseudo-first-order reaction (Wong et al. 2004).

3.7. Data Analysis

The experimental results of antibacterial tests were expressed as mean ± standard deviation (SD) of two replicates. The OriginPro8 software was used to analyzes and draw graphs for all the instrumental analysis. After insertion of organized data, the line and stack lines by Y offset graph line selection was considered.

4. RESULTS AND DISCUSSION

4.1. Thermal Analysis

To obtain a catalytically active, stable, and pure final product, the polyvinyl alcohol (PVA) stabilizing agent that was used during synthesis should be removed. This can be done by calcinating the sample at the DTA-TGA optimized temperature in the furnace. The DTA-TGA analysis was used to select the optimal PVA decomposition temperature (Fig. 4.1). The first small peaks that appeared lower than 140 °C are associated with surface and crystal-adsorbed water dehydration. The other wide exothermic DTA band observed within the 150–210 °C temperature range is associated with the decomposition of the complex formed between the nitrate of the zinc precursor and PVA (Abebe et al. 2020). Lastly, an intense exothermic DTA band was observed within the 300–500 °C temperature range. This intense peak is associated with the pre-formed by product from complex formed decomposition. The instability detected beyond 540 °C is due to the thermal oxidation of carbonized residue (Priya, Basha, and Kumari 2023). Thus, 450 °C is the temperature at which the PVA polymer completely decomposes and gives pure ZnO NPs. This 450 °C was used as calcination temperature to produce pure NPs.

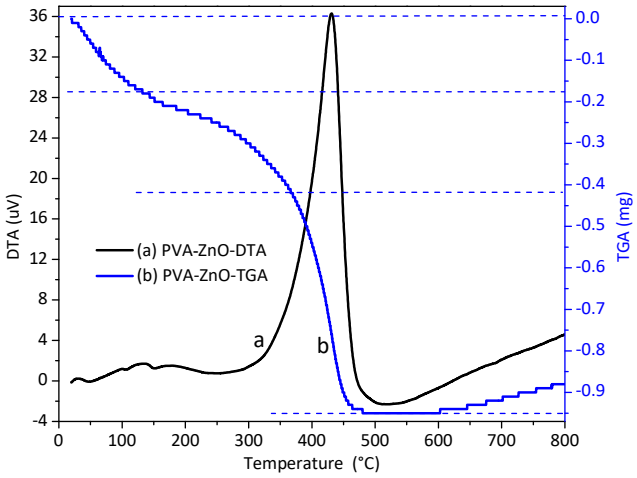

Figure 4. 1: Thermal analysis: DTA-TGA (differential thermal-thermogravimetric analysis) plots of polyvinyl alcohol-zinc precursor complexes before calcinating the sample in the furnace.

4.2 Crystallinity Analysis

4.2.1 Optimization of synthesis temperature and calcination time

The synthesis solution temperature experiment was conducted by taking different temperatures ranging from 30 °C to 90 °C (Fig. 4.2a). In this optimization, the temperature of 50 °C gives a smaller crystallite size. Besides, increasing the calcination time from 30 to 180 min at a fixed temperature of 450 °C resulted in increasing the crystallite size (Figure 4.2b). The obtained result shows that increasing the calcination time from 30 min to 70min results in increased crystallization and crystallite size. The increase in the crystallite size with increasing calcination time confirms the aggregation of the NPs with time and as time increases, the temperature assists in the coalescence process of the NPs. It is observed that the crystalline size at 30 min calcination is 22 nm and for a 1-hour calcination it is 32 nm, Calcination time has no significant effect on crystallite size beyond 70 min. Despite having a slightly larger surface area than 30 min, the 1 hour of calcination time was chosen to maintain confidentiality on the total decomposition of the capping un-combusted agent and other different impurities.

(a)

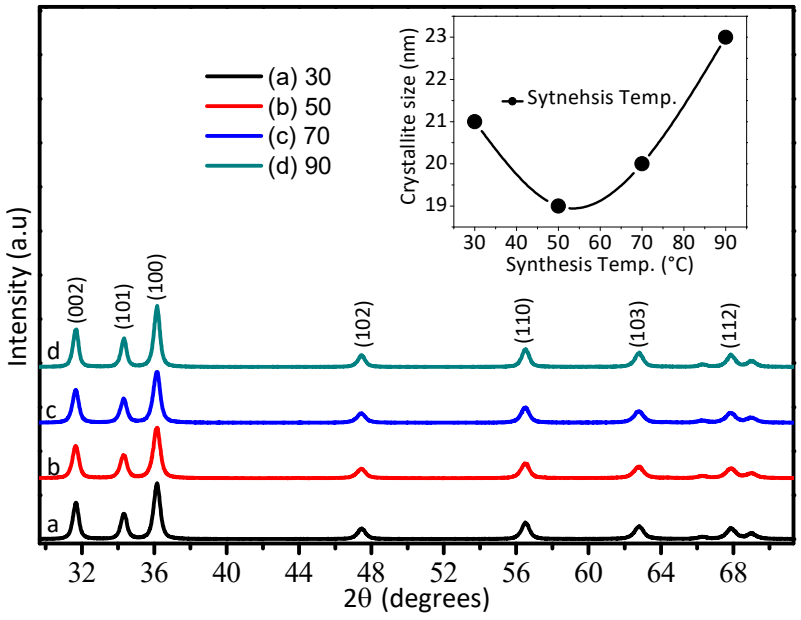

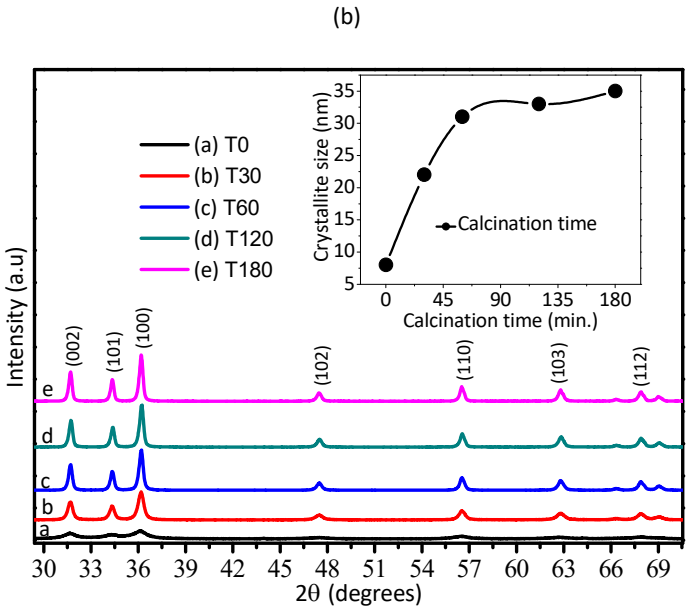

Figure 4. 2: ZnO crystallite size optimization using the X-ray diffraction pattern: (a) synthesis temperature, (b) calcination time.

4.2.2 Comparison of XRD results of calcined and uncalcined NPs and NCs

The un-calcinated ZnO and 15c-zac heterostructures (after drying) show a smaller crystallite size compared to their calcined constituents (Fig. 4.3). However, depending on the pre-photocatalytic test, the 60-minute calcination time was selected as optimum and used for further analysis. Besides, calcinating the material to the optimum time assists in the decomposition of impurities, including the PVA polymer, as well as giving the material good crystallinity.

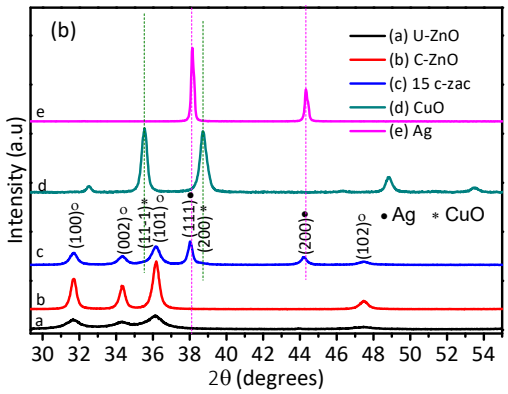

Figure 4. 3: XRD patterns of the uncalcined and calcined, NPs, and nanocomposites.

4.2.3 Optimization of dopant percentage

The dopant percentage optimization shows Ag peak starting from lower dopant percentages of 1% (which means 0.5% for Ag) (Fig. 4.4b). However, the small intensity of CuO-independent peaks was detected only at a higher concentration of 15% (7.5% for copper) and 20 (10% for copper). This indicates that the solubility of copper is better (> 5%) than that of silver. The smaller crystallite size was obtained to be the optimum at 15% dopant concentration.

(a)

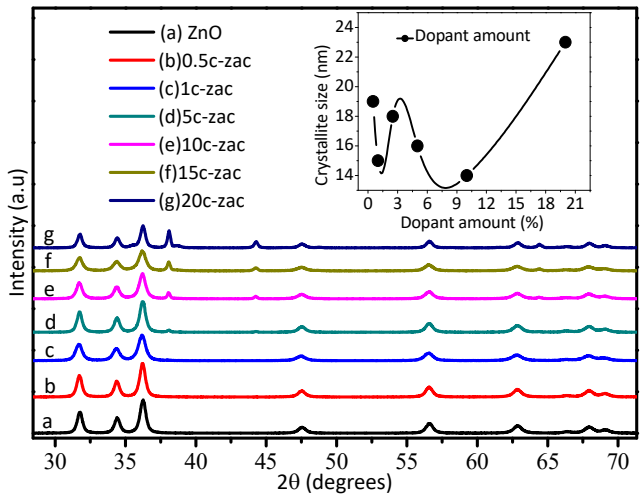

(b)

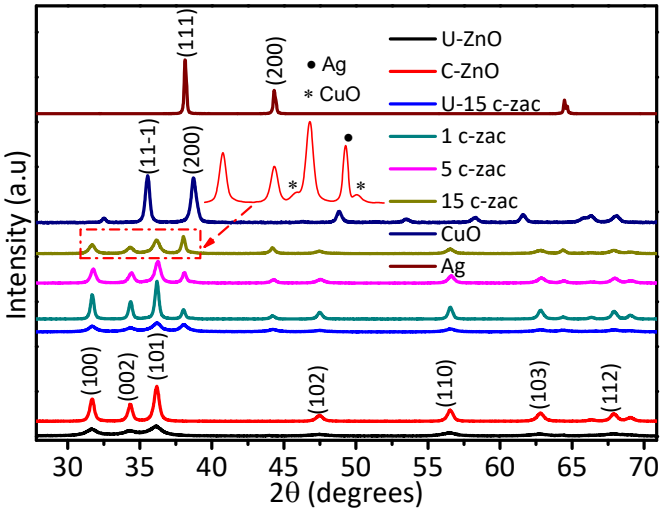

Figure 4. 4: Crystallite size optimization Nanoparticle and nanocomposite using the X-ray diffraction pattern: dopant amount.: (a) the X-ray diffraction patterns of ZnO nanoparticles, and c-zac heterostructures; (b) the magnified views

The Scherrer formula (Equation 1) has been used to calculate the crystallite size of the single NPs and heterostructures. The 2θ values with the respective crystal planes of single ZnO NPs are 31.8 (100), 34 (002), 36 (101), 47.5 (102), 56.6 (110), 62.8 (103), and 67.8 (112), revealing the hexagonal wurtzite structure (JCPDS# 00-036-1451) of ZnO NPs. The XRD pattern of the c-zac heterostructure also has similar 2θ peaks like that in ZnO and an additional three independent silver metal peaks. These three Ag NPs peaks are associated with the fcc structure, which fits with the single Ag 2θ and corresponding crystal plane of 38 (111), 44 (200), and 64 (220) (JCPDS# 00-004-0783). The c-zac heterostructure also has two additional small copper oxide (CuO) independent peaks. These two CuO peaks appeared at 2θ, and the corresponding crystal planes of 35.5 (002, 11-1) and 39 (200, 111) are associated with the monoclinic structure of CuO (JCPDS# 00-048-1548).

Depending on the reaction conditions and synthesis approach, substitutional, interstitial, and heterojunction may occur due to the doping of metal or metal ions. The substitutional and interstitial doping causse's peak shifts on the XRD pattern depending on the ionic radii. Doping silver in the ZnO lattice shifts the Fermi level and creates a deep acceptor level near the host VB (Singh et al. 2019). However, the solubility of silver is very low due to its greater ionic radii, which then form a separate independent crystal (Trang et al. 2020; Wang et al. 2020). Besides, the BUC approach also results in the reduction of silver ions by producing gaseous by-products (Sukhanov et al. 2023). Thus, Ag forms a dominantly heterojunction with ZnO (Schottky contact) than that of its inclusion in the host lattice. The dominance of Schottky contact for Ag and ZnO is also consistent with recent reports (Zulkufile et al. 2023). The ionic radius of the Zn ion (0.74 Å) is smaller than that of the Ag ion (1.26 Å). Thus, inclusion of Ag in the ZnO host lattice results in increasing the unit cell volume and a low-angle shift on the XRD pattern. The radius of the copper ion (0.73 Å) is comparable to that of the zinc (0.74 Å) ion in the tetrahedral structure. Thus, inclusion of copper ions in the ZnO host lattice results in a decrease in unit cell volume and a high angle shift on the XRD pattern (Iribarren, Hernández-Rodríguez, and Maqueira 2014). However, the solubility of silver is very low due to its greater ionic radii. The c-zac heterostructure shows a high angle shift compared to the single ZnO (Fig. 4.5). This shift indicates the domination of copper inclusion in the ZnO lattice. The appearance of silver and copper oxide (CuO) peaks on the XRD patterns indicates the formation of a ZnO/Ag/CuO heterostructure. Thus, a Cu-doped ZnO/Ag/CuO heterostructure is the final product.

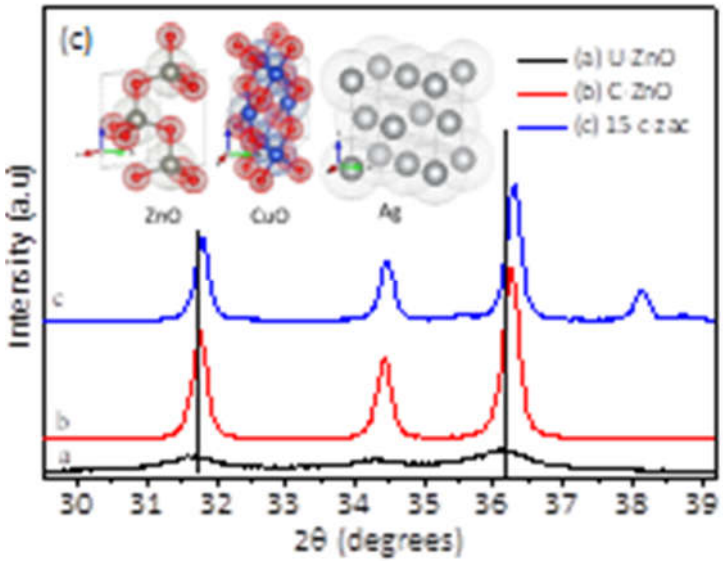

Figure 4. 5: The magnified views of uncalcined and calcined ZnO and calcined c-zac heterostructures.

4.3. Optical Property Analysis

4.3.1 UV–vis diffuse reflectance spectroscopy (DRS)

The optical properties of powder ZnO NPs and c-zac heterostructures were studied by the ultraviolet-visible diffuse reflectance spectroscopy (UV-vis-DRS) technique. The analysis is based on the dispersion of the radiation by a sample (Abebe et al. 2023). The % reflectance versus wavelength in the DRS-UV-vis spectrum is given in Fig. 4.6a. The ZnO NPs and 15c-zac heterostructure show sharp reflection at about 390 nm. This reflection is associated with CB electron and VB hole recombination. It is a distinctive property of the ZnO crystal (Lin et al. 2023). Compared to the ZnO NPs, the 15c-zac showed greater photoactivity (75%, high light absorption property), which is beneficial in visible light utilization. This light absorption ability for the 15c-zac heterostructure is due to the surface plasmon resonance properties of AgNPs (Zulkufile et al. 2023) and mid-gap level creation due to the copper doping. The direct and indirect band gaps of the materials can be determined from the Kubelka-Munk (K-M) function (Fig. 4.6b and c) (Abebe, et al. 2023). This can be done by extrapolating the linear region of the K-M plot towards the x-axis.

The inter-band electron transition mechanism is dependent on the relative positions of the minimum CB and the maximum VB energy level (which are known as crystal momentum (k-vector) values). The change in minimum CB and maximum VB k-factor for the direct band gap semiconductor is zero. While the indirect band gap materials do not have a zero k-

factor value (Correal et al. 2023). The zero change in k-factor for the direct bandgap indicates direct emission of the absorbed energy due to electron-hole recombination. However, this electron-hole recombination process diminished in the indirect materials. This is because the indirect materials have differences in the k factor values. This indicates that the photon-excited electrons and holes get relaxation time for the reduction and oxidation redox reactions. Thus, the reactive oxygen species obtained from the redox reaction are beneficial for applications such as photocatalysis. The obtained direct and indirect bandgap values of ZnO are 3.27 and 3.23 eV, respectively. While the direct and indirect bandgap values for the 15c-zac heterostructure are ZnO are 3.27 and 3.19 eV, respectively. The direct band gap was not affected much by doping, indicating the excitation may occur by indirect transition (Li et al. 2023).

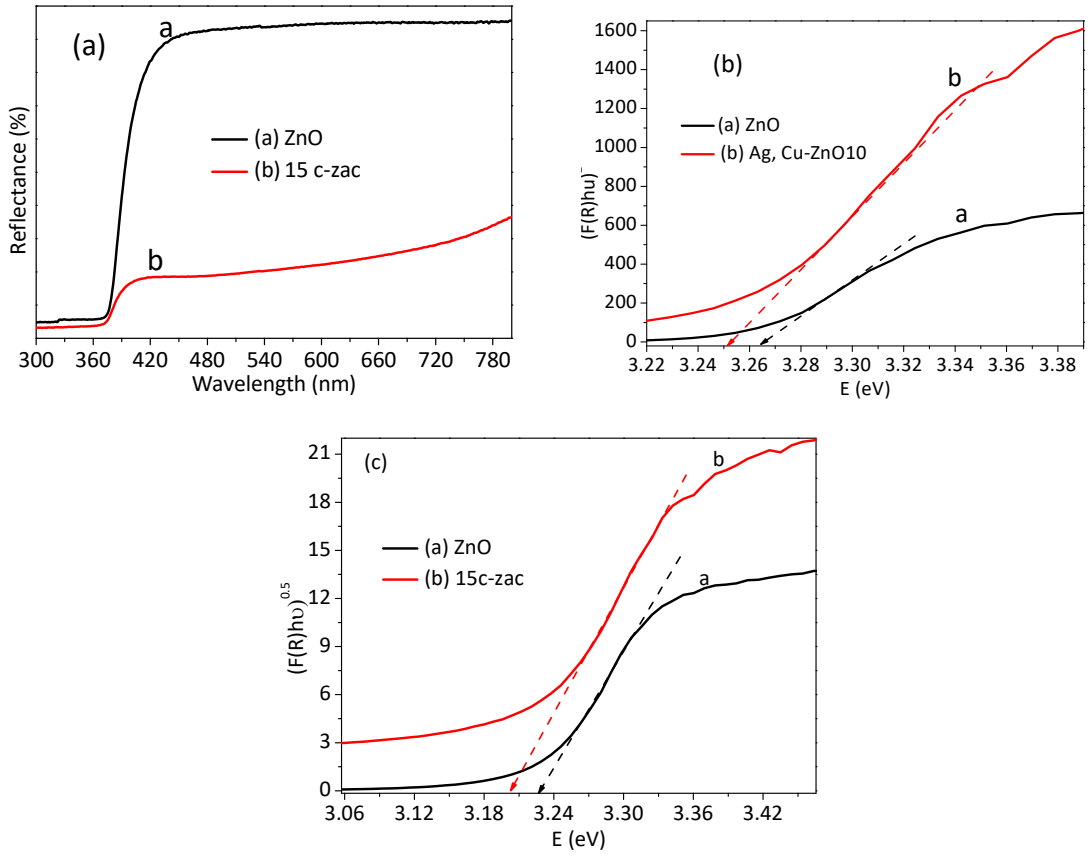

Figure 4. 6: Optoelectronic properties analysis: (a) the DRS-UV-vis spectra; (b and c) th..e respective direct and indirect Kubelka-Munk plots, respectively.

4.3.2 Photo-luminescence (PL) spectroscopy

The optical and luminescence characteristics of ZnO and c-zac heterostructures were also characterized by PL analysis (Fig. 4.7a). The xenon lamp was used as a source at an

excitation wavelength of 325 nm. The common emission band at 394 nm (UV region) is associated with the ZnO-Near Band Edge (NBE) transition as a result of electron-hole recombination. The three emission peaks detected in the visible region are associated with the intrinsic ZnO defects deep-level emission. These emission peaks that are detected at a wavelength of 419 nm, 444 nm, and 486 nm are associated with the violet, blue, and green emission, respectively. The visible emission that occurs during synthesis may be associated with electron donor level Oxygen Vacancy and Zinc interstitials (VO and Zni) or accepter level (VZn and Oi) defects. The accepter level occurred below the CB and the donor level above the VB of the host (Albab et al. 2024). The violet-blue emission is associated with Zni and the host VB transition; the blue emission is associated with Vzn and the host CB transition; green is due to the transition between VO and VZn; and yellow is related to the recombination of holes trapped in Oi and electrons in the CB (Niu et al. 2023; Okeil et al. 2024).

Figures 4.7 b and c show the gaussian-shaped constituents of the deconvoluted plot for ZnO NPs and 15c-zac heterostructure. The intensity of UV emission for doped heterostructure decreased from 46 to 10 arbitrary units. This intensity reduction has a direct relationship with electron-hole recombination hindrance or the presence of charge transfer. This enhanced charge transfer is associated with mid-gap level creation due to copper doping (Divband et al. 2013) as well as heterojunction within the heterostructure interface (ZnO/Ag/CuO) (Mahyoub et al. 2021; Niu et al. 2023). This charge transfer process without recombination has great importance in different applications, such as antibacterial and photocatalysis (Subash et al. 2023; Thabit et al. 2022).

The UV, violet, blue, and green emission for ZnO NPs was observed at about 394, 418, 446, and 460 nm. However, the respective emission peaks for the c-zac heterostructure were observed at 397, 420, 447, and 466 nm, respectively. The UV and blue emissions for the doped heterostructure showed a redshift compared to the ZnO NPs. The observed shift is associated with the host s or p and dopant d state (sp-d) strong exchange interaction (Kopp, Lidegaard, and Magyari 2022; Pashchanka et al. 2011). This host electron interaction with localized unpaired dopant 3d electrons creates a new mid-gap level between the host band gap. Besides, the visible light emission bands were increased compared to the UV emission band for the c-zac heterostructure. The increase in visible emission peaks is associated with an increase in defects as a result of the doped level (Chanda, Gupta, and Vasundhara 2017).

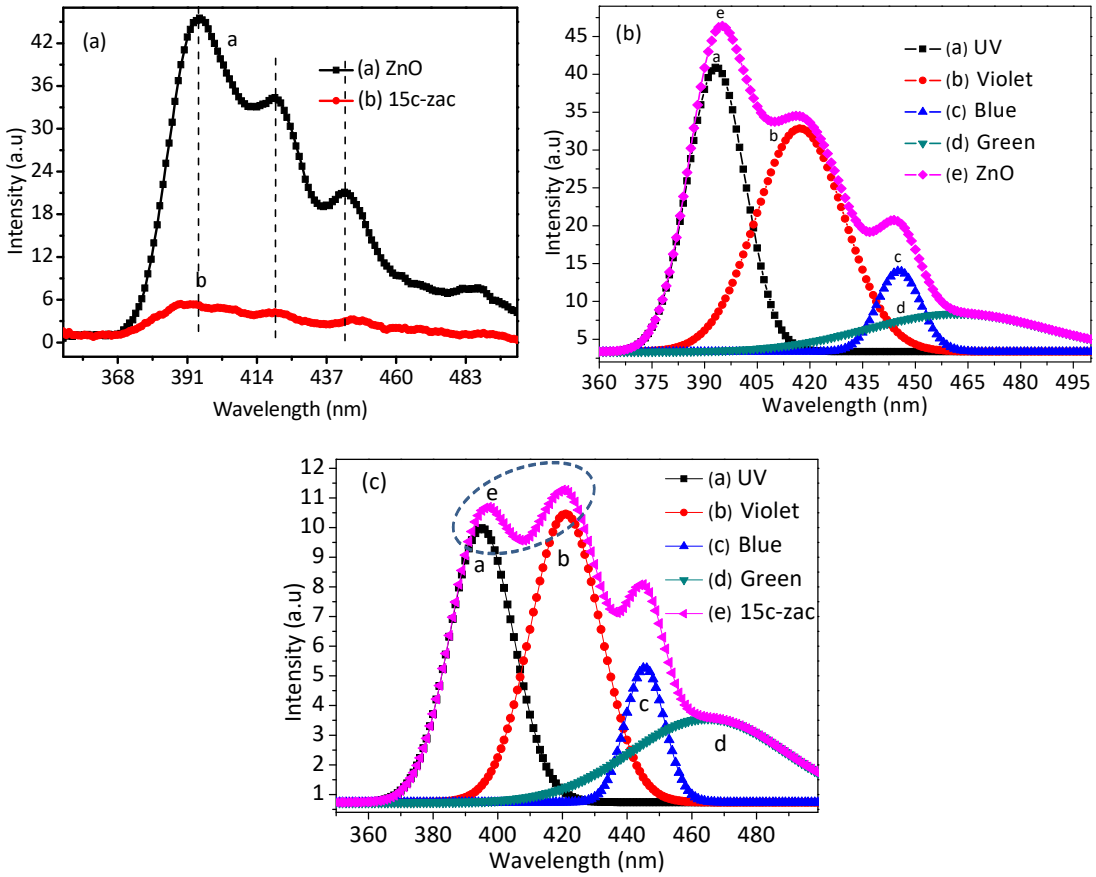

Figure 4. 7: Optical properties of ZnO and c-zac heterostructure: (a) the PL spectra of ZnO and 15c-zac heterostructure; (b and c) are the ZnO and c-zac heterostructure gaussian-shaped constituents of the deconvoluted plots, respectively.

4.4 Fourier-Transform Infrared Spectroscopy (FTIR) Analysis

The metal-oxygen bond and functional group information can be understood from the FT-IR spectroscopic technique. The FTIR analysis was conducted for calcined and uncalcined materials (Fig. 4.8). As usual, the broad bands formed at a wavenumber value of 3350 cm^{-1} (uncalcined) and 3315 cm-1 (calcined) in NPs and heterostructures are due to the vibration of hydroxyl groups. This stretching vibration in the higher wavenumber region is associated with the surface (physiosorbed) and interstitial (chemisorbed) water molecules. The short stretching vibration bands detected in the range of 2425–2260 cm^{-1} are associated with the carbonate peak due to CO_2 absorption. The nanomaterial metal bonded with oxygen (M-O) (Cu-O, Zn-O, or Ag-O) bending vibration bands, which commonly occur below 1000 cm^{-1}, are also observed in both calcined and uncalcined spectra (Silva-neto et al. 2019). Except for slight intensity differences, the bands detected for uncalcined ZnO NPs and c-zac are almost similar. In addition, the bands detected for calcined ZnO NPs and c-zac are also almost

similar. However, there is higher wavenumber spectra shift and greater intensity for calcined NPs and heterostructures compared to the uncalcined ones. This shift is due to the increased rigidity after heat treatment. The rigidity also conforms to the creation of crystalline metal oxide (Prasad et al. 2024) There is one unique bending vibration band detected at 950 cm^{-1} for the c-zac heterostructure, compared to both calcined and uncalcined ZnO NPs. This unique peak is probably associated with the Cu-O bending vibration. Although this unique peak is detected on the calcined c-zac, it is not present on the uncalcined c-zac. There is a higher wavenumber shift for calcined NPs compared to uncalcined NPs and heterostructure, which is due to the metal-oxygen bond stiffness. The distinctive peak was detected at 950 cm^{-1} on the c-zac heterostructure, which is from doped CuO.

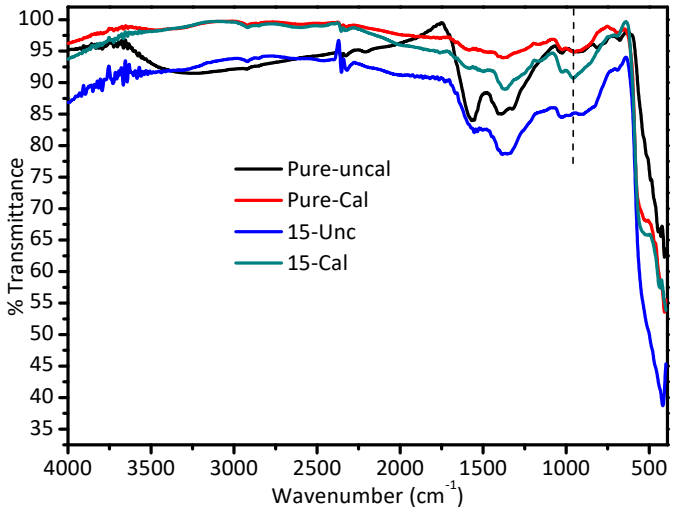

Figure 4. 8: Functional group and metal-oxygen bond properties of uncalcined and calcined ZnO NPs and the c-zac heterostructure.

4.5. Morphological analysis

Once the combustion started at the ignition point of the precursor-PVA complex, the evolution of gaseous by-products started. Then, either a long wire- or spongy-like structure occurs depending on whether the evolution started at one or many points, respectively (Carlos et al. 2020; Nersisyan et al. 2017). The FE-SEM images of ZnO NPs and c-zac heterostructure for this study show a spongy-like structure, which resulted from the evolution of gases from many points, Fig. 4.9 (a) and (b), respectively. Besides, the reactions of gaseous by-products react with metal ions and result in reduction (Nersisyan et al. 2017). The c-zac heterostructure has a greater spongy-like structure compared to ZnO NPs, indicating that the presence of silver and copper salts facilitates the combustion process

more. In addition, the white spots in c-zac indicate reduced silver metal, which is not seen in ZnO. The silver metal within the c-zac heterostructure forms voids or porous regions, and a greater spongy morphology is observed in c-zac structure. This explains the morphological differences between c-zac heterostructures and ZnO NPs. The surface distribution of dopant is a crucial concern for several applications (Abebe and Murthy 2022; Jiang, Gu, and Jiang 2022).

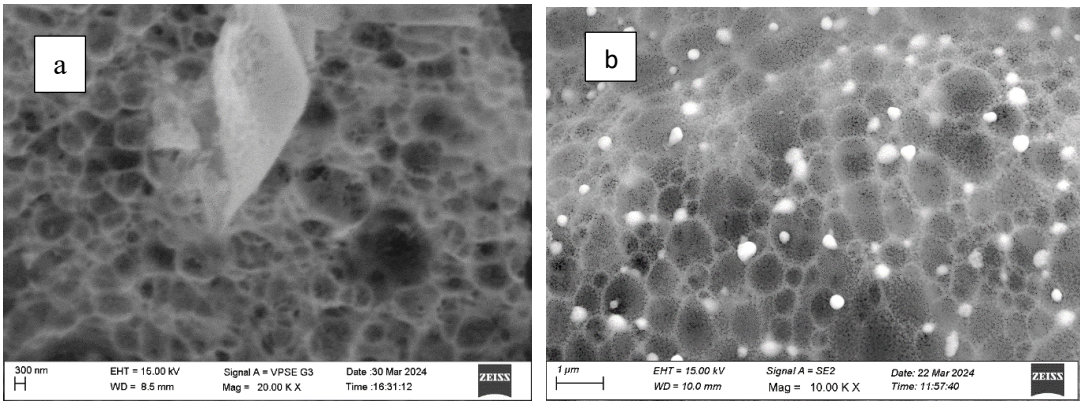

Figure 4. 9: FE-SEM image of (a) ZnO and (b) c-zac

Fig. 4.10 shows EDS compositional and elemental mapping analyses. The EDS-layered image shows a good distribution of copper and silver dopants on the host surface (Fig. 4.10b). The elemental mapping analyses for zinc, copper, silver, and oxygen are depicted in Figs. 4.10 b1–b4, respectively. The elemental mapping image of silver shows white dots (Fig. 4.10 b3). This white dot is also visible on the FE-SEM image with a good distribution, which is probably the reduced silver metal. The presence of only expected elements in the EDX elemental composition analysis also shows material purity. The obtained compositions are also comparable with the amounts added during synthesis (see Fig. 4.10 a_1 and a_2).

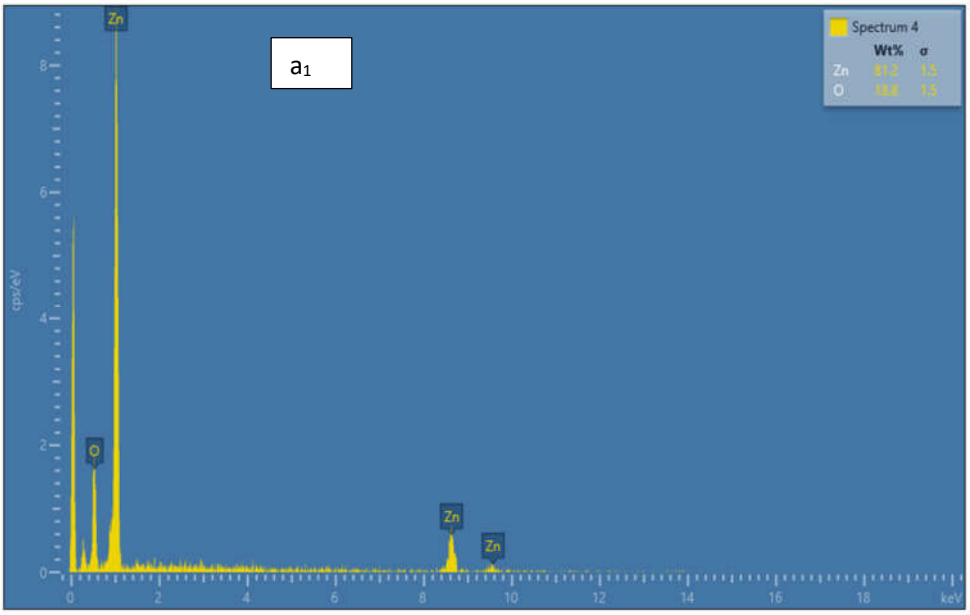
a1
Spectrum 4
Wt% σ
Zn 81.2 1.5
O 18.8 1.5
Zn
O
Zn
Zn
cps/eV
keV

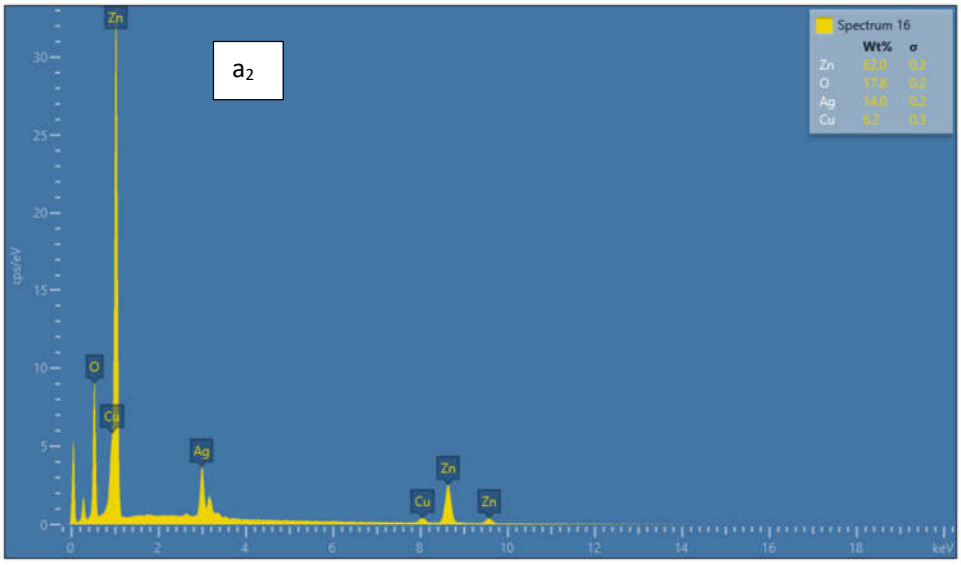
a2
Spectrum 16
Wt% σ
Zn 62.0 0.5
O 17.8 0.2
Ag 14.0 0.2
Cu 6.2 0.3
Zn
O
Cu
Ag
Cu
Zn
Zn
cps/eV
keV

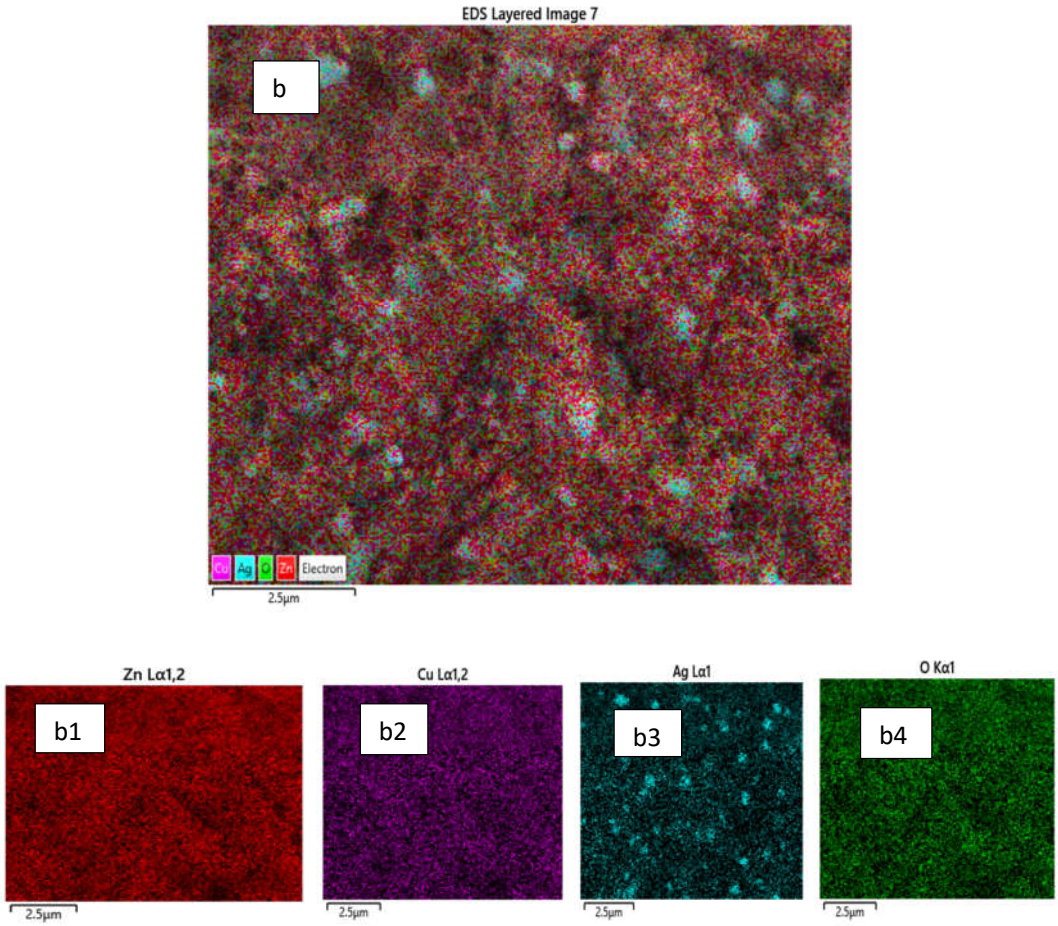

Figure 4. 10: a_1 and a_2 EDX compositional analysis for ZnO NPs and c-zac heterostructure, respectively. (b) EDS layered image; (b1-b4) elemental mapping images of zinc, copper, silver, and oxygen, respectively.

The TEM/HRTEM/SAED images of ZnO and 15c-zac heterostructures are depicted in Fig. 4.11. The TEM images of ZnO and 15c-zac heterostructures are depicted in Fig. 4.11 b_1 and 4.11 a_1, respectively. The morphology shows an agglomeration with a size between 20 and 65 nm. However, 15c-zac heterostructure images show low aggregation properties. The doped heterostructure also shows more additional porosity and channels compared to bare ZnO NPs. This porosity and channel occur during the evolution of gaseous by-products (Nersisyan et al. 2017). Fig. 4.11b_3 and 4.11a_3 show the HRTEM analyses for ZnO NPs and doped heterostructure, respectively. The d-spacing value of 0.264 nm on a single ZnO HRTEM image matches the (002) plane of the ZnO crystallite. The d-spacing values of 0.280 and 0.25 nm on the c-zac heterostructure are associated with ZnO and Ag crystals. They correspond to the hexagonal (002) plane of ZnO and the spherical (111) plane of Ag

crystallites. The existence of Ag crystals indicates the presence of local contact (Schottky contact) between ZnO and Ag crystallites (Pham 2020) Fig. 4.11b_2 and 4.11a_2 show the SAED images for ZnO and c-zac heterostructures, respectively. The ring and white spots in the SAED image show the crystalline nature of the materials.

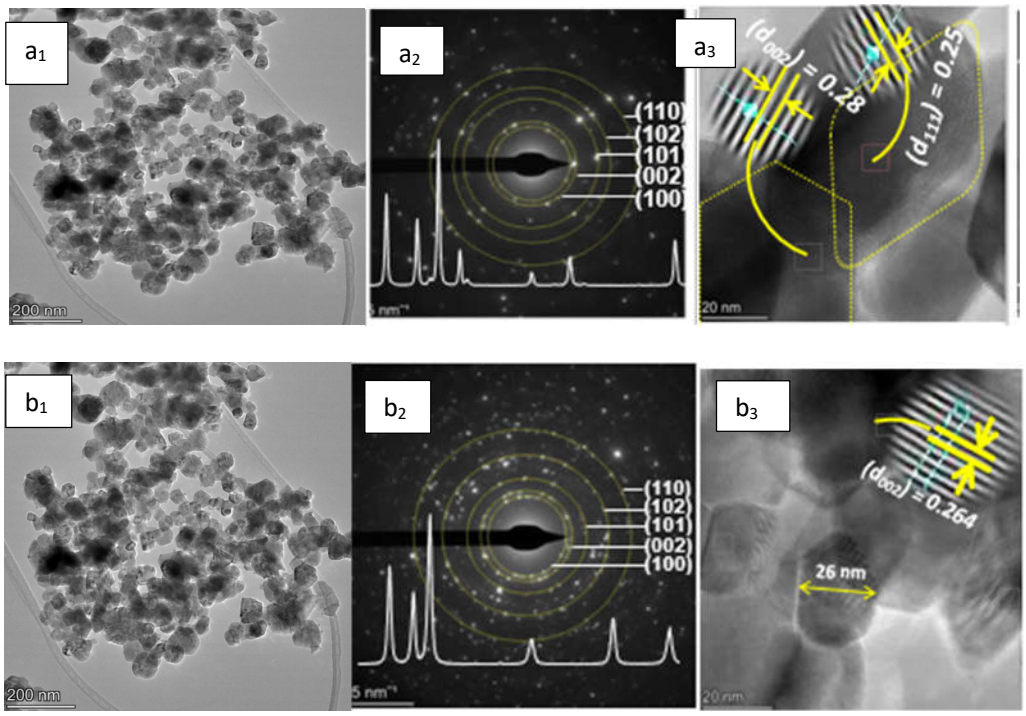

Figure 4.1 1: (a1-a3) TEM image, SAED ring and HRTEM of c-zac heterostructure, and (b1-b3) TEM image, SAED ring and HRTEM of ZnO NPs.

4.6. Antibacterial activities of synthesized NPs, and NCs

The antibacterial activity of ZnOu, ZnOc, c-zacu and C-zacc was examined using the disc diffusion method and different bacterial strains that included two gram-positive (*S. aureus* ATCC25923 and *S. pyogenes* ATCC19615) and two gram-negative (*E. coli* ATCC25923 and *P. aeruginosa* ATCC27853) at different concentrations (70,60, 50, and 40 mg/mL). Ciprofloxacin (25 µg/mL) and DMSO (10%) were used as a positive control (PC) and negative control (NC), respectively. The results are shown in Table 1 and Figure 4.12 for all tests. In general, all the calcined and uncalcined ZnO and c-zac showed antibacterial activity against both the gram-positive and gram-negative bacterial strains tested with dose-dependency manner, which is the zone of inhibition increased with increasing concentrations except for uncalcined sample against gram negative bacteria especially E-coli. The standard ciprofloxacin (at 25 µg) has the antibacterial activities within the range of 27.5 ±0.7 to

25.5±0.7, DMSO has no activity (0mm) on whole tested bacterial strain and it was used as solvent in samples serial dilution. For *E. coli, S. aureus, P. aeruginosa* and *S. pyogenes* measurable zone of inhibition (MZI) values varied from 6±0.7 to 16.5±0.7, 6.5±0.7 to 16±1.41, 8.5 ±0.7 to 15 ±0.7 and 7.5±0.7 to 17.5 ±0.7, respectively. ZnO nanoparticle and c-zac showed better activity on Gram-positive bacteria than Gram-negative bacteria. The variations in structural components between Gram-positive and Gram-negative bacteria may account for the differences in their susceptibility to antibacterial agents. The structural elements of lipopolysaccharides in the outer phospholipid membrane of Gram-negative bacteria contribute to the impermeability of their cell walls to antimicrobial substances(Pop et al. 2020). In contrast, Gram-positive bacteria possess an outer peptidoglycan layer that renders their cell walls more permeable to antimicrobial agents compared to the lipopolysaccharide layer in Gram-negative bacteria. Consequently, the structural complexity of the cell walls in Gram-negative bacteria surpasses that of Gram-positive bacteria. As a result, Gram-negative bacteria demonstrate lower susceptibility to antimicrobial substances compared to Gram-positive bacteria(Tavares et al. 2020).

The crystallite size of the ZnOu and c-zacu are very small, which is appropriate to penetrate the membrane of bacteria and cause unicellular damage to the bacteria probably due to the size effect; the smaller the size of the NPs, the higher their antibacterial activity. Nanocomposite have also disturb biological processes and cause damage to the DNA, as previously reported(Dan et al. 2023). In support of this result, it is also confirmed by the PL and DRS results (Fig.4.6 and Fig 4.7, respectively), which show high surface defects that indicate roughness, which can generate ROS and cause damage to the bacteria's cells (Xie et al. 2023). It was also observed that NCs show significant toxicity to the bacterial strains. According to a previous report(Raju et al. 2022), NCs have the potential to penetrate the cells of microorganisms as well as accumulate in the cell. Doping of ZnO NPs has been shown to impart a synergy effect and improve the antibacterial property (Mirzaeifard et al. 2020). We also observed a significant enhancement of antibacterial activity by c-zac compared to ZnO NPs alone.

The bactericidal activity by the generation of ROS follows a highly oxidizing agent generation process, which means the direct interaction of NPs and NCs led to damage the cell wall and generates ROS inside. The generated hydroxyl radicals, a highly oxidizing agent, deactivate the bacteria (Adhikari et al. 2015; Zhang et al. 2014). The release of ions through the dissolution of the NPs is also the other bactericidal activity mechanism. Once

the smaller nanoscale size ions are released, they can enter through cell cytoplasm that has a greater size than the NPs and generate ROS through the Fenton reaction by interacting with the mitochondria that inhibit DNA replication (Cui et al. 2016; V. Jagadeeswar et al. 2023). Therefore, the NPs interaction with the bacterial cell or/and release of ions due to ZnO, CuO and Ag dissolution, resulting in the generation of hydroxyl radicals by the Fenton reaction, can be the probable bacterial deactivation mechanism.

Table 1. Antibacterial activity (zone of inhibition) of ZnO, and 15c-zac

Measurable zone of inhibition (MZI) of ZnO Np (mm)				
Concentration (mg/mL)	E. coli	P. aeruginosa	S. aureus	S. pyogenes
70	7.5±0.7	7 ±0.7	14.5±0.7	14±0
60	7 ±0.7	6.5 ±0.7	12.5±0	12.5±0.7
50	6.5 ±0.7	6±0.7	6.5±0.7	11.5±0.7
40	6 ±0.7	6 ±0.7	7±0	9.5±0.7
PC	25 ±0.7	26±0.7	25.5±0.7	26±0
NC	6	6	6	6
Measurable zone of inhibition (MZI) of uncalcined ZnO Np (mm)				
Concentration (mg/mL)	E. coli	P. aeruginosa	S. aureus	S. pyogenes
70	8.5±0.7	7.5 ±0.7	16±1.41	16±0
60	7.5±0.7	7.5±0.7	14.5±0.7	13.5±0.7
50	7.5±0.7	6.5 ±0.7	12.5±0.7	9.5±0.7
40	6.5±0.7	6 ± 0.7	6.5±0.7	7.5±0.7
PC	26.5±0.7	25.5 ±0	25±0.7	26.5±0.7
NC	6	6	6	6
Measurable zone of inhibition (MZI) of 15c-zac (mm)				
Concentration (mg/mL)	E. coli	P. aeruginosa	S. aureus	S. pyogenes
70	16.5±0.7	14.5 ±0.7	15.5 ±0.7	17.5 ±0.7
60	14 ±1.41	13.5 ±0.7	13.5 ±0.7	15.5 ±0.7
50	13.5 ±0.7	10.5 ±0.7	11.5 ±0.5	13.5 ±0.7
40	7.5 ±0.7	8.5 ±0.7	6.7 ±0.7	9.5 ±0.7
PC	26.5 ±0.7	26 ±1.41	27.5 ±0.7	26 ±1.41
NC	0	0	0	0
Measurable zone of inhibition (MZI) of uncalcined 15c-zac (mm)				
Concentration (mg/mL)	E. coli	P. aeruginosa	S. aureus	S. pyogenes
70	14.5 ±0.7	15 ±0.7	15.5 ±0.7	17.5 ±0.7
60	15 ±0	13.5 ±0.7	13 ±0	15.5 ±0.7
50	13.5 ±0.7	11 ±0	7.5 ±0.7	13.5 ±0.7
40	12 ±0	9.5 ±0.7	7 ±0	9.5 ±0.7
PC	25.5 ±0.7	26 ±0.7	25.5 ±0.7	26 ±1.41
NC	0	0	0	0

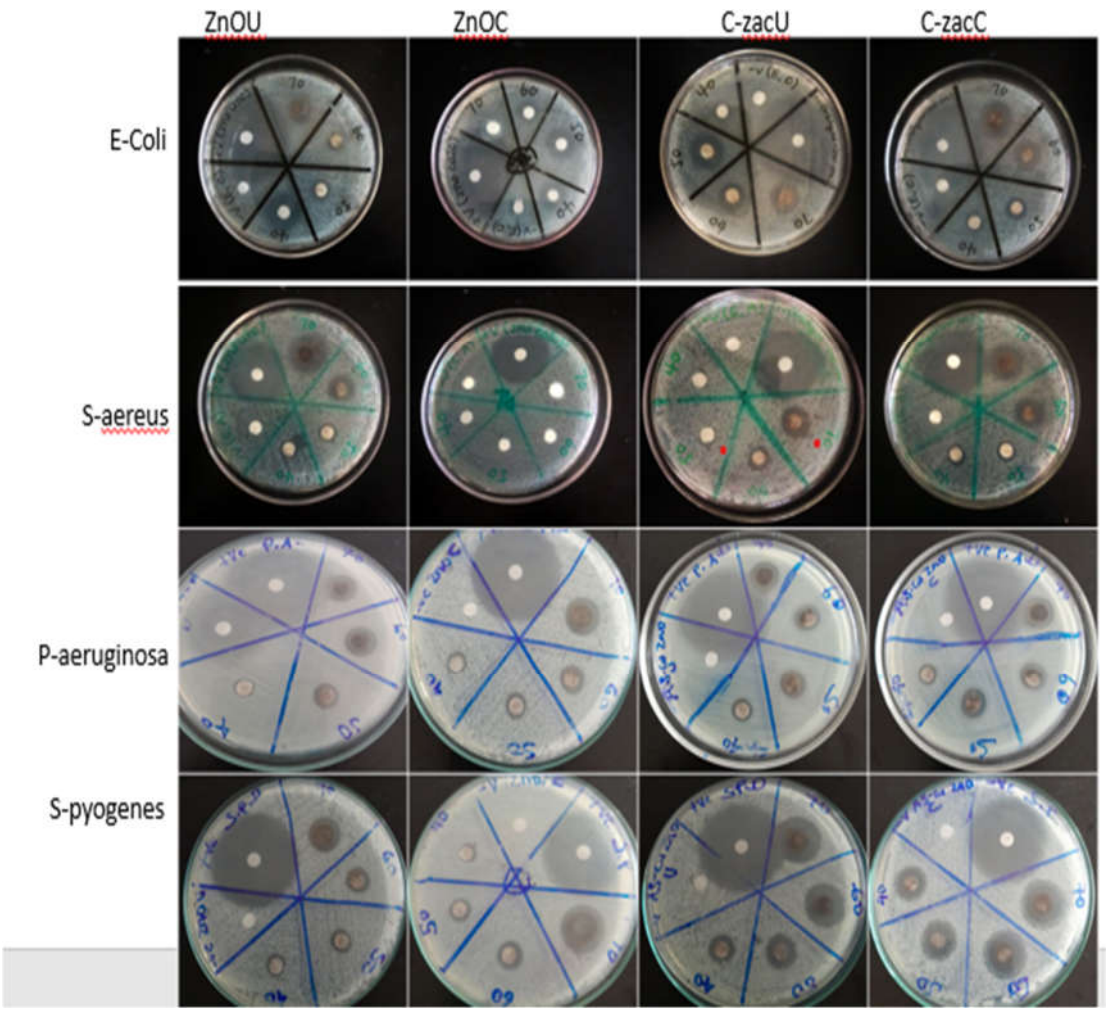

Figure 4.1 2: Zone of inhibition of ZnOu, ZnOc, C-zac, and C-zacC

Figure 4.1 3: shows the zone of inhibitions of the different nanomaterials along with the NC and PC.The result is against two gram-negative (*E. coli and P. aeruginosa*) and two gram-positive (*S. aureus and S. pyogenes*). The numbers on the plates indicate concentration of respective samples (70, 60, 50 and 40 mg/mL),

4.6. Photocatalytic Activity

More surface defects on the porous NCs increase photocatalytic degradation activity and light absorption efficiency (Suresh et al. 2023). It is common knowledge that exposing a ZnO photocatalyst to radiation of sufficient energy results in the formation of electron and hole pairs on the surface of the photocatalyst. The electrons interact with oxygen on the reduction of half-reaction ions to produce superoxide radicals, consequently producing the highly oxidizing agent, hydroxide radicals. Besides, the hole interacts with water in the oxidation half-reaction and generates more hydroxide radicals. However, the band potential of the photocatalyst determines whether these two reactions take place. When pollutants are adsorbed, the hydroxide radical oxidizing agent interacts with them and converts them to harmless minerals. However, an issue with electron-hole recombination may arise when using a single ZnO as a photocatalyst. This recombination issue, which is more enunciated inside the nanoscale expand, diminishes their quantum capability and may as well trigger incredibly needed reactions and have proposals for the dispersal of brilliant imperativeness (Uma et al. 2023). Doping and the creation of an interface between two or more metal oxide semiconductors are two of the many methods discovered to enhance the photocatalysts' capacity for charge transfer (Rajakumari, Mohandoss, and Sureshkumar 2023).

The pollutant degradation properties of synthesized ZnO NPs, Ag- and Cu-ZnO, and 15c-zac were tested on MB-D, as shown in Fig. 4.13. ZnO shows less potential (k = 0.0041 min-1) compared to all the other heterostructures. The c-zac heterostructure exhibits better activity (k = 0.023 min-1) compared to other heterostructures. This is due to the synergistic effect of CuO and Ag crystals. Additionally, the change in optoelectrical properties is due to copper doping. Fig 4.13 shows (a) ZnO NPs, (b) Ag-ZnO, (c) Cu-ZnO, and (d) c-zac heterostructure at an initial MB concentration of 10 ppm and a catalyst amount of 20 mg; (e and f) the Ct/Co and lnCt/Co versus time plots of the NPs and heterostructures. As the result on the graph indicates the c-zac heterostructure has greater photocatalytic performance due to its improved opto electric properties and synergistic effect.

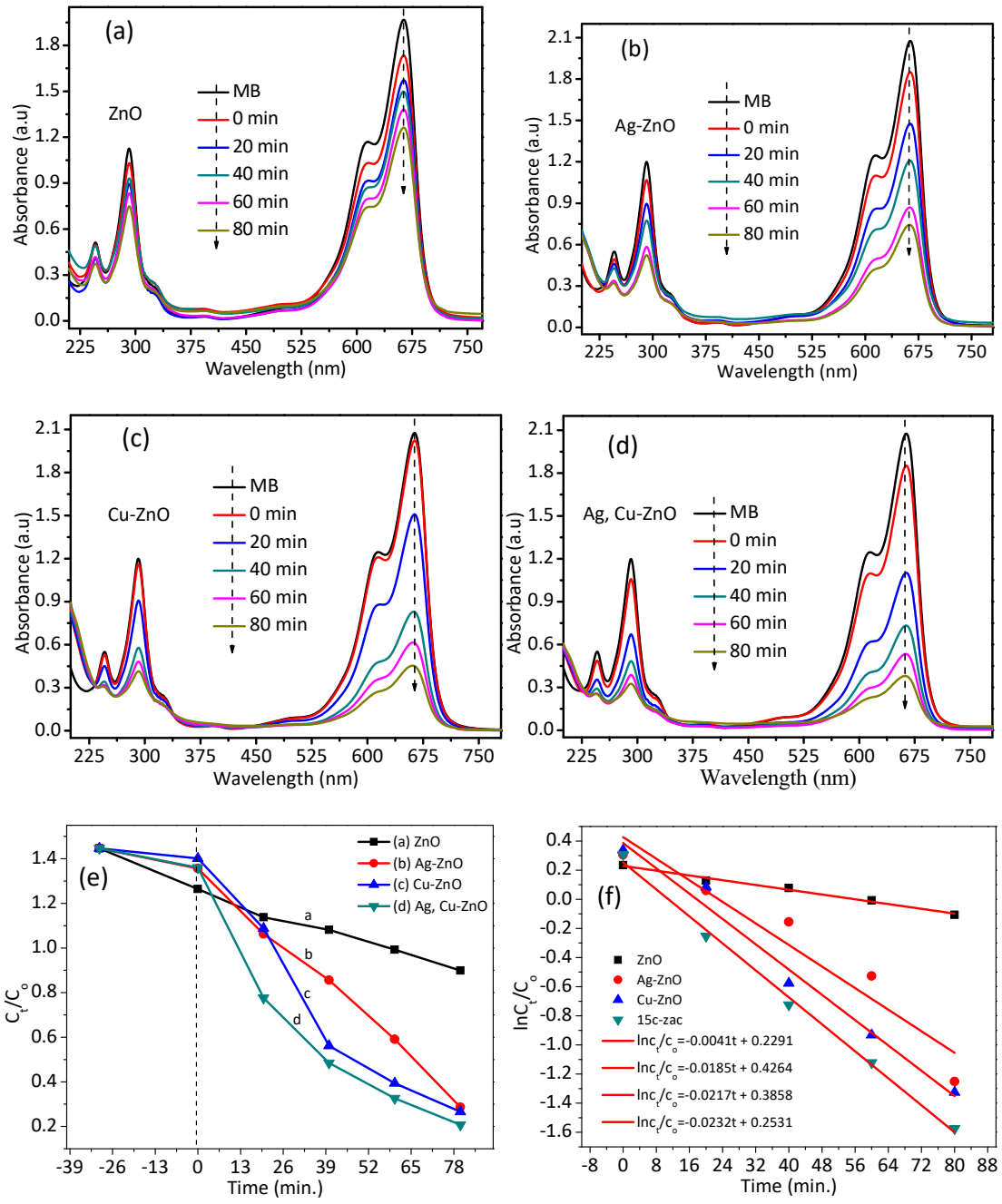

Figure 4.14: The absorbance vs. wavelength plots of (a) ZnO NPs, (b) Ag-ZnO, (c) Cu-ZnO, and (d) c-zac heterostructure (e) the Ct/Co vs time (f) lnCt/Co versus time plots of the NPs and heterostructures

The photodegradation process was optimized for the effect of pH (in the range of 4-9) and catalyst dose (1-30 mg) as discussed in sections 4.6.1 and 4.6.2.

4.6.1. Dosage Effect

The catalyst dose was optimized by taking different dosage amounts of 1, 10, 20, and 30 mg. The optimum catalyst dosage was obtained to be 20 mg (Fig. 4.14). The lower photocatalytic potential at lower catalyst amounts is associated with the scarcity of active sites for MB-D sorption. In addition, the lower potential at a higher dosage of 30 mg is associated with turbidity, which prevents light from reaching the surface. Besides, high catalyst amounts also result in decreasing catalyst active sites due to agglomeration in solution (Mirzaeifard et al. 2020). Sorption of the MB-D on the surface of the catalyst was the first step in its photocatalytic degradation. Then, migration of the photon-induced electron and hole on the surface and reaction with adsorbed MB-D occur. A catalyst amount of 20 mg has greater photocatalytic performance. A lower catalyst amount of 1 and 10 mg lacks active sites for sorption. At a high catalyst amount of 30 mg, the catalyst protects the light from reaching the adsorbed methylene blue dye.

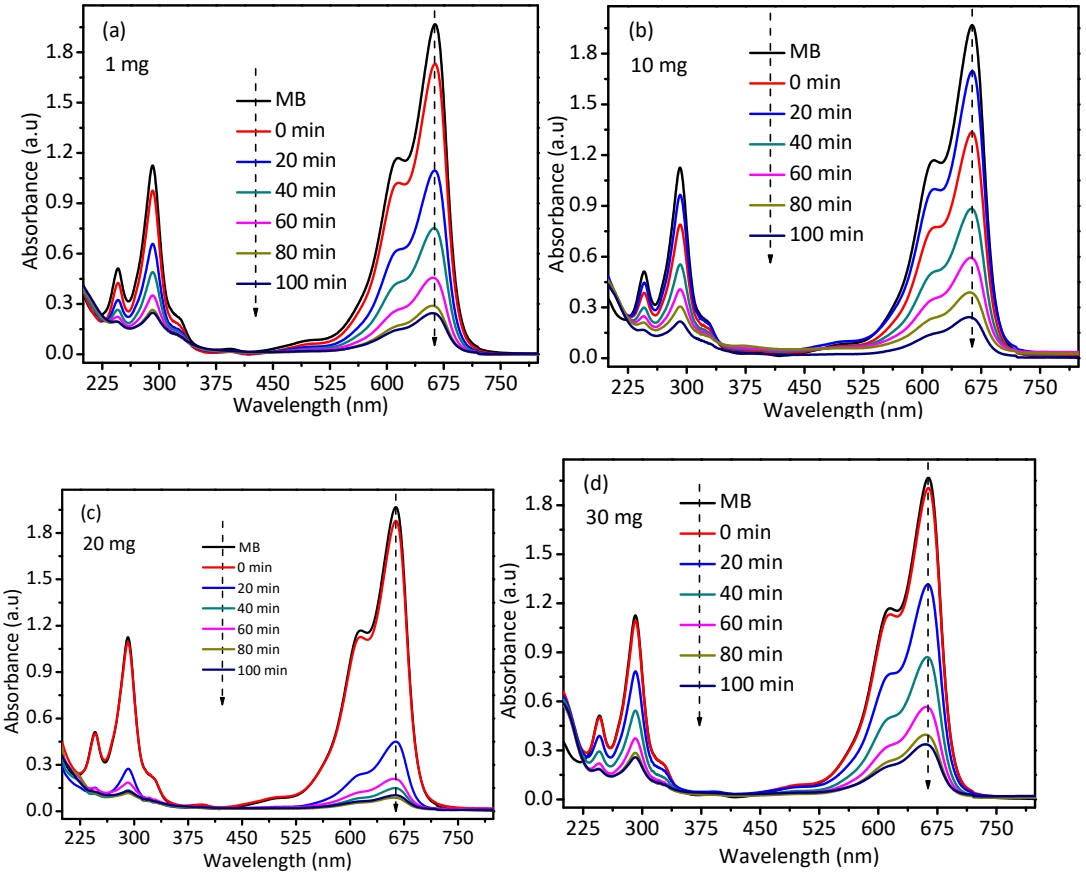

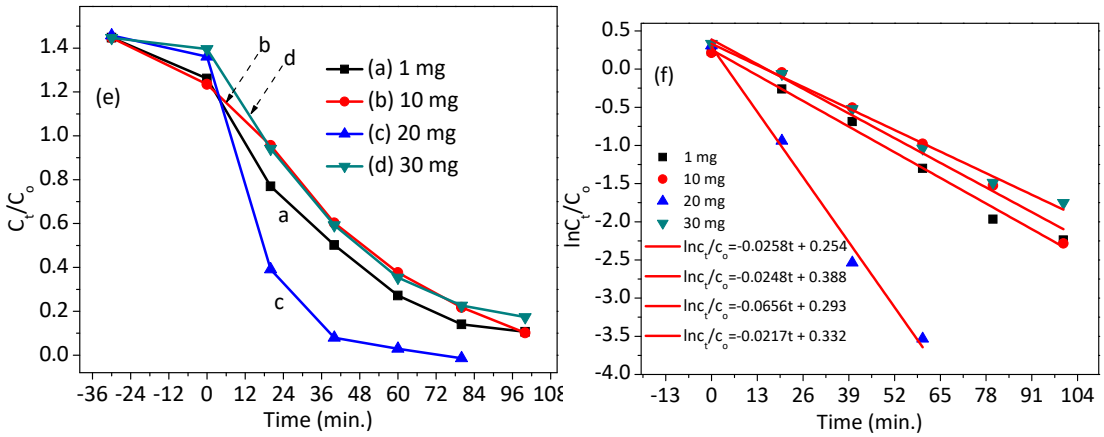

Figure 4.15: the absorbance vs. wavelength plots of the c-zac heterostructure at an initial MB concentration of 10 ppm, an optimized solution pH of 9, and different catalyst amounts (a) 1 mg (b) 10 mg (c) 20 mg and (d) 30 mg; (e and f) Ct/Co and lnCt/Co versus time plots of the NPs and heterostructures, respectively.

4.6.2. pH Effect

To control the sorption and electrostatic interaction between the catalysts and MB-D solution, pH optimization has been conducted. Fig. 4.15 shows effects of pH and Ct/Co and lnCt/Co versus time plots of the NPs and heterostructures on the photodegradation of MB-D. The basic region (pH of 9) showed greater photocatalytic performance due to the attractive MB and catalyst electrostatic interaction effects. In the acidic solution (pH = 4), the catalyst is surrounded by positive hydrogen ions. The electrostatic repulsive interaction between the positively charged MB-D and catalyst protects the dye's sorption on the catalyst's surface in acidic media. Since there is no photocatalytic reaction without sorption, less photocatalytic activity was observed (k = 0.020 min^{-1}). At a neutral pH of 7, the c-zac heterostructure catalyst degradation activity is relatively better than that at an acidic pH (k = 0.023 min^{-1}). As the solution pH increased to 9, the degradation potential increased significantly (k = 0.065 min^{-1}). At an alkaline pH range of 9, the catalyst surface is surrounded by negatively charged hydroxyl ions. Then, the negatively charged catalyst surface and positively charged MB-D electrostatically attract each other.

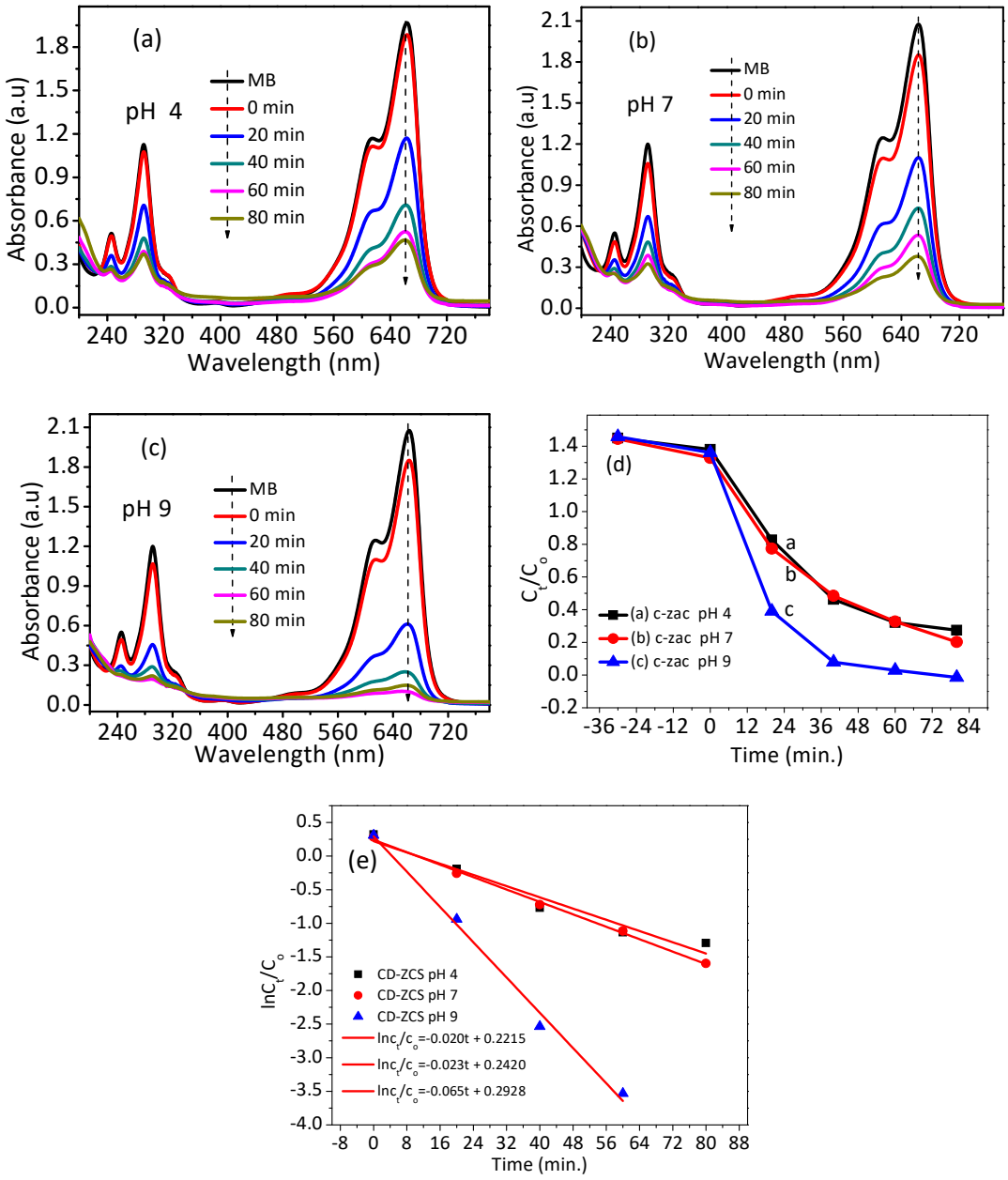

Figure 4.16: the absorbance vs. wavelength plots of c-zac heterostructures at an initial MB concentration of 10 ppm, a catalyst amount of 20 mg, and different pH values: (a) 4 (b) 7 and (c) 9; (d and e) Ct/Co and lnCt/Co versus time plots of the NPs and heterostructures, respectively.

4.6.3 Comparison of photocatalytic activities of calcined and uncalcined nanomaterials

As indicated in the XRD pattern analysis interpretation, the crystallite size for the uncalcined 15c-zac heterostructure was about 8 nm. This smaller crystallite size and greater surface area

resulted in greater sorption of the dye on the catalyst surface. Of course, this greater sorption property in dark for the uncalcined ZnO and 15c-zac heterostructures has been conformed, as shown in Fig. 4.16 b and 4.16 d. With this information, the photocatalytic activities of calcined and uncalcined ZnO NPs and the c-zac heterostructure were tested at an optimised pH of 9. The photocatalysis time was also extended to 100 minutes to see the change in detail. However, the test showed that the potential for calcined ZnO NPs ($k = 0.028\ min^{-1}$) and c-zac heterostructure ($k = 0.067\ min^{-1}$) is much greater than that of uncalcined ZnO NPs ($k = 0.015\ min^{-1}$) and c-zac heterostructure ($k = 0.012\ min^{-1}$). The decrease in photocatalysis potential for the uncalcined materials is due to a lack of crystallinity and the blockage of the nanocrystals from light by the uncalcined impurities. Besides, to see the effects of dopant amount, the calcined 5c-zac heterostructure was also tested. Here, the 5c-zac heterostructure showed lower activity ($k = 0.017\ min^{-1}$) than the 15c-zac heterostructure, as shown in Fig. 4.16e at an initial MB concentration of 10 ppm, a catalyst amount of 20 mg, and a solution pH of 9. The 15c-zac heterostructure has greater performance compared to both ZnO NPs and the 5c-zac heterostructure. The calcined NPs and heterostructure showed greater photocatalytic performance, probably due to the greater crystallinity effects.

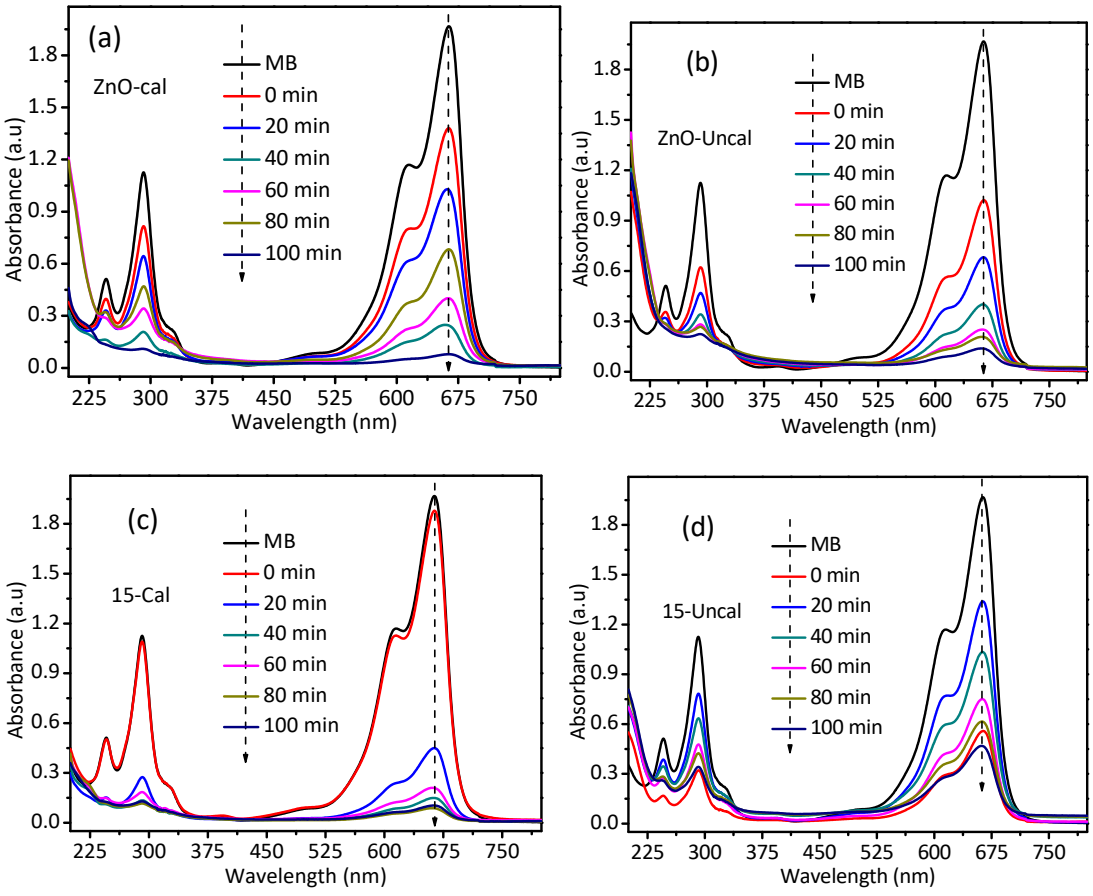

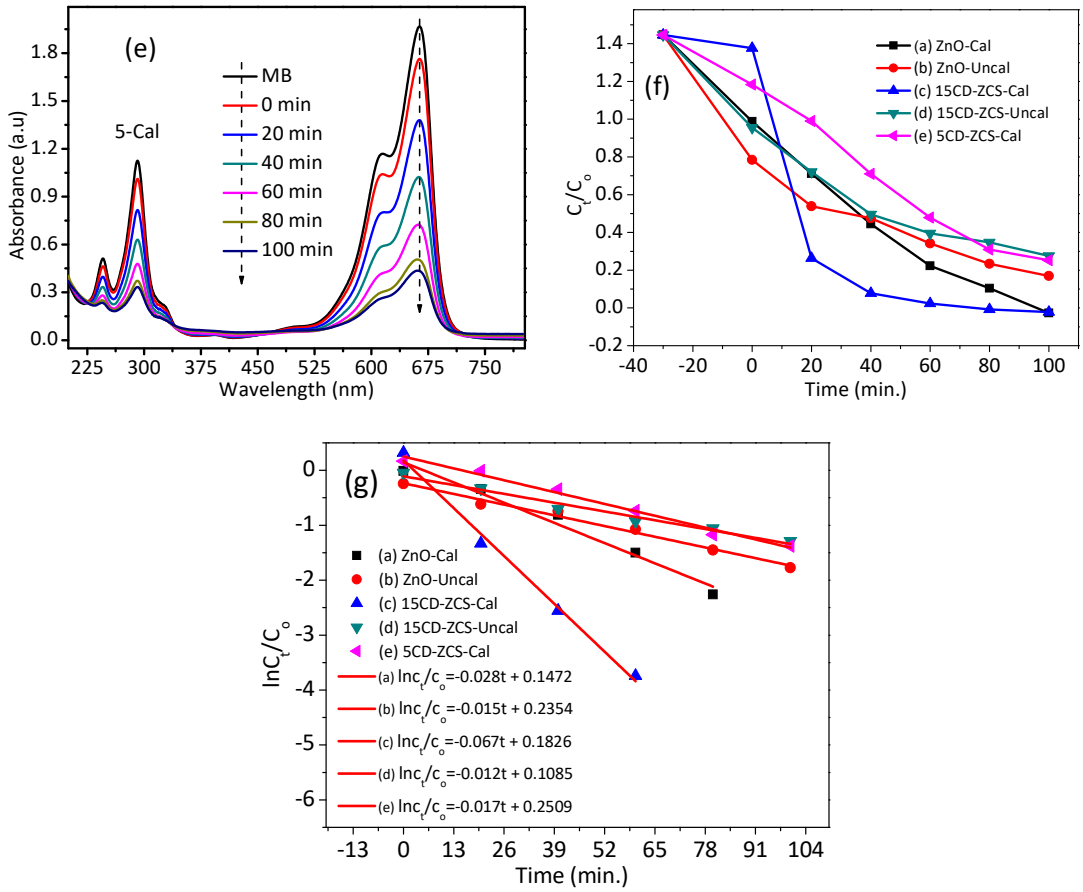

Figure 4.17: The absorbance vs. wavelength plots of calcined and uncalcined (a and b) ZnO NPs and (c and d) 15c-zac and (e) calcined 5c-zac heterostructures (f and g) Ct/Co and lnCt/Co versus time plots of the NPs and heterostructures, respectively.

Conclusions

Here, the porous heterostructure is effectively synthesized. 1.00 g of PVA at a fixed precursor concentration of 0.25 M/100 mL was obtained to be the optima. Besides, the synthesis temperature of 50 °C and the calcination time of 1 hour were optimized and fixed. The Cu-doped ZnO and ZnO/Ag/CuO formations were confirmed from the HRTEM image and XRD pattern analysis. The obtained crystallite size was found to be10–25 nm. The particle size was found to be within the range of 40–75 nm. The porosity observed on the FESEM image is associated with gaseous by-product evolution. The solubility of copper dopant was found to be much better than that of silver. The optical property change for ZnO is associated with copper 3d mid-gap state formation and heterojunction. The mid-gap level is a result of host-dopant sp-d strong exchange interaction. The c-zac heterostructure ($k = 0.067\ min^{-1}$) showed enhanced methylene blue degradation potential compared to single ZnO ($k = 0.0041\ min^{-1}$). This greater potential is due to the enhanced optoelectrical and charge transfer properties. All the calcined and uncalcined ZnO and c-zac had promising antibacterial activity against *E. coli* (ATCC 25923), *P. aeruginosa* (ATCC 27823), *S. aureus* (ATCC 25923), and *S. pyogenes* (ATCC 11778). This is due to its small average crystalline size, uniform spherical shape, and large surface region, which creates electronic effects, and these effects can increase the binding strength of the nanoparticles with the bacteria cell membrane. The bactericidal effect of NPs was found to be the same yet slightly higher for Gram-positive bacteria compared to the Gram-negative bacteria. It is due to the difference in the structural composition of Gram-positive and Gram-negative bacteria. Among synthesized sample c-zac showed maximum zone of inhibition on *S. pyrogens* (17.5±0.7) at concentration of 70 mg/mL. The uncalcined ZnO showed high inhibition on *E-coli* 6±0.7 mm at a concentration of 50 mg/mL.

Recommendations

The following recommendation ought to be considered for future work:

- ✓ The BUC synthesis approach was found to be useful for the preparation of composite materials in the current study. After further testing and refinement, this technology should be used to degrade dye in the textile industry. In addition, it should also be used as an antibiotic in the pharmaceutical industry.
- ✓ Since the doping chemistry is not easily understandable, we recommend further studies using advanced techniques. Confirming the presence of real doping or/and local heterojunction using advanced analytical techniques X-ray Absorption Spectroscopy (XAS) and Scanning Tunneling Microscopy (STM): provide more information about the presence and distribution of dopant atoms within a nanomaterial.
- ✓ Biological activities (antifungal, anticancer, cytotoxic) will be needed in the future. Additionally, in vitro antimicrobial studies on other resistant clinical isolates of pathogenic bacterial and fungal organisms are recommended.

RESEARCH FUND ACKNOWLEDGEMENT

This research is funded by Adama Science and Technology University under grant number ASTU/SM-R/999/24.

References

Abebe, Buzuayehu, Bontu Kefale, and Dereje Tsegaye Leku. 2023. “Nanocomposites for 4-Nitrophenol Reduction :” 4523–29. doi: 10.1039/d2ra07845g.

Abebe, Buzuayehu, H. C. Ananda Murthy, Enyew Zerefa, and Yeshaneh Adimasu. 2020. “PVA Assisted ZnO Based Mesoporous Ternary Metal Oxides Nanomaterials : Synthesis , Optimization , and Evaluation of Antibacterial Activity PVA Assisted ZnO Based Mesoporous Ternary Metal Oxides Nanomaterials : Synthesis , Optimization , and Evaluation of Antibacterial Activity.”

Abebe, Buzuayehu, Dereje Tsegaye, Chaluma Sori, Ravikumar Chunchana kuppe Renuka Prasad, and H. C. Anand. Murthy. 2023. “Cu/CuO-Doped ZnO Nanocomposites via Solution Combustion Synthesis for Catalytic 4-Nitrophenol Reduction.” *ACS Omega* 8(10):9597–9606. doi: 10.1021/acsomega.3c00141.

Abebe, Buzuayehu, Enyew A. Zereffa, and H. C. Ananda Murthy. 2021. “Synthesis of Poly(Vinyl Alcohol)-Aided ZnO/Mn 2 O 3 Nanocomposites for Acid Orange-8 Dye Degradation: Mechanism and Antibacterial Activity.” *ACS Omega* 6(1):954–64. doi: 10.1021/acsomega.0c05597.

Adhikari, Sangeeta, Aditi Banerjee, Neerugatti KrishnaRao Eswar, Debasish Sarkar, and Giridhar Madras. 2015. “Photocatalytic Inactivation of E. Coli by ZnO–Ag Nanoparticles under Solar Radiation.” *RSC Advances* 5(63):51067–77. doi: 10.1039/C5RA06406F.

Agarwal, D. C., U. B. Singh, Srashti Gupta, Rahul Singhal, P. K. Kulriya, Fouran Singh, A. Tripathi, Jitendra Singh, U. S. Joshi, and D. K. Avasthi. 2019. “Enhanced Room Temperature Ferromagnetism and Green Photoluminescence in Cu Doped ZnO Thin Film Synthesised by Neutral Beam Sputtering.” *Scientific Reports* 9(1):6675. doi: 10.1038/s41598-019-43184-9.

Ahmed, Warish, Kerry A. Hamilton, Aldo Lobos, Bridie Hughes, Christopher Staley, Michael J. Sadowsky, and Valerie J. Harwood. 2018. “Quantitative Microbial Risk Assessment of Microbial Source Tracking Markers in Recreational Water Contaminated with Fresh Untreated and Secondary Treated Sewage.” *Environment International* 117(May):243–49. doi: 10.1016/j.envint.2018.05.012.

Al-Zaqri, Nabil, K. Umamakeshvari, V. Mohana, A. Muthuvel, and Ahmed Boshaala.

2022. “Green Synthesis of Nickel Oxide Nanoparticles and Its Photocatalytic Degradation and Antibacterial Activity.” *Journal of Materials Science: Materials in Electronics* 33(15):11864–80. doi: 10.1007/s10854-022-08149-1.

Albab, Muh Fadhil, Muhammad Jahandar, Yong Hyun Kim, Yong Ki Kim, Myunghun Shin, Adi Prasetio, Soyeon Kim, and Dong Chan Lim. 2024. “High-Performance Semi-Transparent Organic Solar Cells Driven by the Dipole-Controlled Optoelectrical Response of Bilateral Self-Assembled Monolayer Strategy.” *Nano Energy* 121(December 2023):109219. doi: 10.1016/j.nanoen.2023.109219.

Alqadi, M. K., A. B. Migdadi, F. Y. Alzoubi, H. M. Al-Khateeb, and Ahmad A. Almasri. 2022. “Influence of (Ag–Cu) Co-Doping on the Optical, Structural, Electrical, and Morphological Properties of ZnO Thin Films.” *Journal of Sol-Gel Science and Technology* 103(2):319–34. doi: 10.1007/s10971-022-05785-1.

Alshehri, Abdulmohsen Ali, and Maqsood Ahmad Malik. 2019. “Biogenic Fabrication of ZnO Nanoparticles Using Trigonella Foenum-Graecum (Fenugreek) for Proficient Photocatalytic Degradation of Methylene Blue under UV Irradiation.” *Journal of Materials Science: Materials in Electronics* 30(17):16156–73. doi: 10.1007/s10854-019-01985-8.

Aravind, M., M. Amalanathan, and M. Sony Michael Mary. 2021. “Synthesis of TiO2 Nanoparticles by Chemical and Green Synthesis Methods and Their Multifaceted Properties.” *SN Applied Sciences* 3(4):1–10. doi: 10.1007/s42452-021-04281-5.

Areerob, Yonrapach, Ju Yong Cho, Won Kweon Jang, and Won-chun Oh. 2018. “Enhanced Sonocatalytic Degradation of Organic Dyes from Aqueous Solutions by Novel Synthesis of Mesoporous Fe3O4-Graphene/ZnO@SiO2 Nanocomposites.” *Ultrasonics Sonochemistry* 41(August 2017):267–78. doi: 10.1016/j.ultsonch.2017.09.034.

Bakken, Kristine, Ola Gjønnes Grendal, and Mari Ann Einarsrud. 2023. “In Situ Characterisation for Studying Nucleation and Growth of Nanostructured Materials and Thin Films during Liquid-Based Synthesis.” *Journal of Sol-Gel Science and Technology* 105(2):596–605. doi: 10.1007/s10971-022-05974-y.

Barui, Ayan K., Rajesh Kotcherlakota, and Chitta R. Patra. 2018. *Biomedical Applications of Zinc Oxide Nanoparticles*. Elsevier Inc.

Bechambi, Olfa, Manel Chalbi, Wahiba Najjar, and Sami Sayadi. 2015. “Photocatalytic Activity of ZnO Doped with Ag on the Degradation of Endocrine Disrupting under UV Irradiation and the Investigation of Its Antibacterial Activity.” *Applied Surface Science* 347:414–20. doi: 10.1016/j.apsusc.2015.03.049.

Binazadeh, Mojtaba, Jamal Rasouli, Samad Sabbaghi, Seyyed Mojtaba Mousavi, Seyyed Alireza Hashemi, and Chin Wei Lai. 2023. “An Overview of Photocatalytic Membrane Degradation Development.” *Materials* 16(9):2522–65. doi: 10.3390/ma16093526.

Bukhari, Aysha, Irfan Ijaz, Ezaz Gilani, Ammara Nazir, Hina Zain, and Ramsha Saeed. 2021. “Green Synthesis of Metal and Metal Oxide Nanoparticles Using Different Plants ’ Parts for Antimicrobial Activity and Anticancer Activity : A Review Article.”

Buonsanti, Raffaella, Vincenzo Grillo, Elvio Carlino, Cinzia Giannini, Tobias Kipp, Roberto Cingolani, and Pantaleo Davide Cozzoli. 2008. “Nonhydrolytic Synthesis of High-Quality Anisotropically Shaped Brookite TiO 2 Nanocrystals.” *Journal of the American Chemical Society* 130(33):11223–33. doi: 10.1021/ja803559b.

Cai, Hua, Peipei Liang, Zhigao Hu, Liqun Shi, Xu Yang, Jian Sun, Ning Xu, and Jiada Wu. 2016. “Enhanced Photoelectrochemical Activity of ZnO-Coated TiO2 Nanotubes and Its Dependence on ZnO Coating Thickness.” *Nanoscale Research Letters* 11(1). doi: 10.1186/s11671-016-1309-9.

Cai, Zhengqing, Youmin Sun, Wen Liu, Fei Pan, Peizhe Sun, and Jie Fu. 2017. “An Overview of Nanomaterials Applied for Removing Dyes from Wastewater.” *Environmental Science and Pollution Research* 24(19):15882–904. doi: 10.1007/s11356-017-9003-8.

Carlos, Emanuel, Rodrigo Martins, Elvira Fortunato, and Rita Branquinho. 2020. “Solution Combustion Synthesis : Towards a Sustainable Approach for Metal Oxides.” 9099–9125. doi: 10.1002/chem.202000678.

Chahar, Mamta, Sarita Khaturia, Har Lal Singh, Vijendra Singh Solanki, Neha Agarwal, Dipak Kumar Sahoo, Virendra Kumar Yadav, and Ashish Patel. 2023. “Recent Advances in the Effective Removal of Hazardous Pollutants from Wastewater by Using Nanomaterials—A Review.” *Frontiers in Environmental Science* 11(August). doi: 10.3389/fenvs.2023.1226101.

Chanda, Anupama, Shipra Gupta, and M. Vasundhara. 2017. “Study of Structural , Optical and Magnetic Properties.” *RSC Advances* 7:50527–36. doi: 10.1039/C7RA08458G.

Chauhan, Ankush, Ritesh Verma, Swati Kumari, Anand Sharma, Pooja Shandilya, Xiangkai Li, Khalid Mujasam Batoo, Ahamad Imran, Saurabh Kulshrestha, and Rajesh Kumar. 2020. “Photocatalytic Dye Degradation and Antimicrobial Activities of Pure and Ag-Doped ZnO Using Cannabis Sativa Leaf Extract.” *Scientific Reports* 10(1):1–16. doi: 10.1038/s41598-020-64419-0.

Ciocci, Paolo, Dimitrios Valavanis, Gabriel N. Meloni, Jean-François Lemineur, Patrick R. Unwin, and Frédéric Kanoufi. 2023. “Optical Super-Localisation of Single Nanoparticle Nucleation and Growth in Nanodroplets.” *ChemElectroChem* 10(9). doi: 10.1002/celc.202201162.

Communication, Short, and The Detection. 2016. “I Nternational J Ournal of V Eterinary S Cience.” *International Journal of Veterinary Science* 5(1):44–47.

Copaciu, Florina, Virginia Coman, Mihaela Vlassa, and Ocsana Opriş. 2012. “Determination of Some Textile Dyes in Wastewater by Solid Phase Extraction Followed by High-Performance Thin-Layer Chromatography.” *Journal of Planar Chromatography - Modern TLC* 25(6):509–15. doi: 10.1556/JPC.25.2012.6.4.

Correal, Sergio, Daniel Hernández-Gómez, Andrea Steffania Esquivel, Alexander Cardona-Rodríguez, Andreas Reiber, Yenny Hernandez, Rafael González-Hernández, and Juan Gabriel Ramírez. 2023. “Tuning Electronic and Magnetic Properties through Disorder in V2O5 Nanoparticles.” *Scientific Reports* 13(1):1–9. doi: 10.1038/s41598-023-32642-0.

Cui, Jianghu, You Liang, Desong Yang, and Yingliang Liu. 2016. “Facile Fabrication of Rice Husk Based Silicon Dioxide Nanospheres Loaded with Silver Nanoparticles as a Rice Antibacterial Agent.” *Scientific Reports* 6(1):21423. doi: 10.1038/srep21423.

Dan, Sasan, Hamidreza Bagheri, Alireza Shahidizadeh, and Hassan Hashemipour. 2023. “Performance of Graphene Oxide/SiO2 Nanocomposite-Based: Antibacterial Activity, Dye and Heavy Metal Removal.” *Arabian Journal of Chemistry* 16(2):104450. doi: 10.1016/j.arabjc.2022.104450.

Divband, B., M. Khatamian, G. R. Kazemi Eslamian, and M. Darbandi. 2013. “Applied Surface Science Synthesis of Ag / ZnO Nanostructures by Different Methods and

Investigation of Their Photocatalytic Efficiency for 4-Nitrophenol Degradation." *Applied Surface Science* 284:80–86. doi: 10.1016/j.apsusc.2013.07.015.

Dutta, Anushree, Anumita Paul, and Arun Chattopadhyay. 2016. "The Effect of Temperature on the Aggregation Kinetics of Partially Bare Gold Nanoparticles." *RSC Advances* 6(85):82138–49. doi: 10.1039/c6ra17561a.

Ebrahimi, Roya, Khosro Hossienzadeh, Afshin Maleki, Reza Ghanbari, Reza Rezaee, Mahdi Safari, Behzad Shahmoradi, Hiua Daraei, Ali Jafari, Kaan Yetilmezsoy, and Shivaraju Harikaranahalli Puttaiah. 2019. "Effects of Doping Zinc Oxide Nanoparticles with Transition Metals (Ag, Cu, Mn) on Photocatalytic Degradation of Direct Blue 15 Dye under UV and Visible Light Irradiation." *Journal of Environmental Health Science and Engineering* 17(1):479–92. doi: 10.1007/s40201-019-00366-x.

Emmanuel, Stephen Sunday, Ademidun Adeola Adesibikan, and Oluwaseyi Damilare Saliu. 2023. *Phytogenically Bioengineered Metal Nanoarchitecture for Degradation of Refractory Dye Water Pollutants: A Pragmatic Minireview*. Vol. 37.

Espitia, Paula Judith Perez, Nilda de Fátima Ferreira Soares, Jane Sélia dos Reis Coimbra, Nélio José de Andrade, Renato Souza Cruz, and Eber Antonio Alves Medeiros. 2012. "Zinc Oxide Nanoparticles: Synthesis, Antimicrobial Activity and Food Packaging Applications." *Food and Bioprocess Technology* 5(5):1447–64. doi: 10.1007/s11947-012-0797-6.

Gebauer, Denis, and Helmut Cölfen. 2011. "Prenucleation Clusters and Non-Classical Nucleation." *Nano Today* 6(6):564–84. doi: 10.1016/j.nantod.2011.10.005.

Gui, Jing, Muwei Ji, Jiajia Liu, Meng Xu, Jiatao Zhang, and Hesun Zhu. 2015. "Phosphine-Initiated Cation Exchange for Precisely Tailoring Composition and Properties of Semiconductor Nanostructures: Old Concept, New Applications." *Angewandte Chemie* 127(12):3754–58. doi: 10.1002/ange.201410053.

Gunawan, A. A., A. Wills, A. Mkhoyan, M. G. Thomas, and D. J. Norris. 2012. "Imaging 'Invisible' Dopant Atoms in Semiconductor Nanocrystals." *Microscopy and Microanalysis* 18(S2):298–99. doi: 10.1017/S1431927612003340.

Guo, Jiaojiao, and Cheng Peng. 2015. "Synthesis of ZnO Nanoparticles with a Novel Combustion Method and Their C2H5OH Gas Sensing Properties." *Ceramics*

International 41(2):2180–86. doi: 10.1016/j.ceramint.2014.10.017.

GuruSampath Kumar, A., Xuejin Li, Yu Du, Youfu Geng, and Xueming Hong. 2020. "UV-Photodetector Based on Heterostructured ZnO/(Ga,Ag)-Co-Doped ZnO Nanorods by Cost-Effective Two-Step Process." *Applied Surface Science* 509:144770. doi: 10.1016/j.apsusc.2019.144770.

Hachem, Kadda, Mohammad Javed Ansari, Raed Obaid Saleh, Hamzah H. Kzar, Moaed E. Al-Gazally, Usama S. Altimari, Shaymaa Abed Hussein, Halah T. Mohammed, Ali Thaeer Hammid, and Ehsan Kianfar. 2022. "Methods of Chemical Synthesis in the Synthesis of Nanomaterial and Nanoparticles by the Chemical Deposition Method: A Review." *BioNanoScience* 12(3):1032–57. doi: 10.1007/s12668-022-00996-w.

Ijaz, Mohsin, Maria Zafar, Atif Islam, Sumera Afsheen, and Tahir Iqbal. 2020. "A Review on Antibacterial Properties of Biologically Synthesized Zinc Oxide Nanostructures." *Journal of Inorganic and Organometallic Polymers and Materials* 30(8):2815–26. doi: 10.1007/s10904-020-01603-9.

Iribarren, A., E. Hernández-Rodríguez, and L. Maqueira. 2014. "Structural, Chemical and Optical Evaluation of Cu-Doped ZnO Nanoparticles Synthesized by an Aqueous Solution Method." *Materials Research Bulletin* 60:376–81. doi: 10.1016/j.materresbull.2014.08.059.

Jagadeeswar, V., V. Dhinesh, S. Mohana Roopan, and E. James Jabaseelan Samuel. 2023. "Plant Extract-Mediated Synthesis of Ag-Doped ZnO: Eco-Friendly Nanomaterial for Environmental Restoration, Microbial Inhibition, Cell Toxicity, Antioxidant Potential, and Sensing." *Colloid Journal* 85(5):827–45. doi: 10.1134/S1061933X23600513.

Jiamprasertboon, Arreerat, Lappawat Ngamwongwan, Weradesh Sangkhun, and Atipong Bootchanont. 2023. "Controllable Synthesis of Nanostructured Bismuth Vanadate Thin Films as an Efficient Catalyst for Photoelectrochemical Water Splitting." (January). doi: 10.1039/D3NJ01456H.

Johnson, Luke, Dominic M. Gray, Edyta Niezabitowska, and Tom O. McDonald. 2021. "Multi-Stimuli-Responsive Aggregation of Nanoparticles Driven by the Manipulation of Colloidal Stability." *Nanoscale* 13(17):7879–96. doi: 10.1039/d1nr01190a.

Jun, Young-wook, Jin-sil Choi, and Jinwoo Cheon. 2006. "Shape Control of Semiconductor and Metal Oxide Nanocrystals through Nonhydrolytic Colloidal

Routes." *Angewandte Chemie International Edition* 45(21):3414–39. doi: 10.1002/anie.200503821.

Kawsar, Md, Md Sahadat Hossain, Newaz Mohammed Bahadur, and Samina Ahmed. 2024. "Synthesis of Nano-Crystallite Hydroxyapatites in Different Media and a Comparative Study for Estimation of Crystallite Size Using Scherrer Method, Halder-Wagner Method Size-Strain Plot, and Williamson-Hall Model." *Heliyon* 10(3):e25347. doi: 10.1016/j.heliyon.2024.e25347.

KESKİN, Banu Hümeyra, and Şükrü ÖKSÜZ. 2024. "Comparison of Rapid Antibiotic Susceptibility Test Method Directly from Blood Culture Bottle with Standard Disc Diffusion Method." *Düzce Tıp Fakültesi Dergisi* (X):1–7. doi: 10.18678/dtfd.1379737.

Khan, Mohammad Mansoob, Mohammad Hilni Harunsani, Ai Ling Tan, Mirabbos Hojamberdiev, Yap Ai Poi, and Norhayati Ahmad. 2020. "Antibacterial Studies of ZnO and Cu-Doped ZnO Nanoparticles Synthesized Using Aqueous Leaf Extract of Stachytarpheta Jamaicensis." *BioNanoScience* 10(4):1037–48. doi: 10.1007/s12668-020-00775-5.

Khort, Alexander, Jonas Hedberg, Nanxuan Mei, Valentin Romanovski, Eva Blomberg, and Inger Odnevall. 2021. "Corrosion and Transformation of Solution Combustion Synthesized Co, Ni and CoNi Nanoparticles in Synthetic Freshwater with and without Natural Organic Matter." *Scientific Reports* 11(1):7860. doi: 10.1038/s41598-021-87250-7.

Kopp, Tine Iskov, Øjvind Lidegaard, and Melinda Magyari. 2022. "Hormone Therapy and Disease Activity in Danish Women with Multiple Sclerosis: A Population-based Cohort Study." *European Journal of Neurology* 29(6):1753–62. doi: 10.1111/ene.15299.

Kulyk, B., B. Sahraoui, V. Figà, B. Turko, V. Rudyk, and V. Kapustianyk. 2009. "Influence of Ag, Cu Dopants on the Second and Third Harmonic Response of ZnO Films." *Journal of Alloys and Compounds* 481(1–2):819–25. doi: 10.1016/j.jallcom.2009.03.117.

Laganà, A., G. Visalli, F. Corpina, M. Ferlazzo, A. D. I. Pietro, and A. Facciolà. 2023. "Antibacterial Activity of Nanoparticles and Nanomaterials: A Possible Weapon in

the Fight against Healthcare-Associated Infections." *European Review for Medical and Pharmacological Sciences* 27(8):3645–63. doi: 10.26355/eurrev_202304_32151.

Lee, Sang Hun, and Bong Hyun Jun. 2019. "Silver Nanoparticles: Synthesis and Application for Nanomedicine." *International Journal of Molecular Sciences* 20(4):1–23. doi: 10.3390/ijms20040865.

Li, Dan, and Richard B. Kaner. 2006. "Shape and Aggregation Control of Nanoparticles : Not Shaken , Not Stirred." (7):968–75.

Li, Jinhua, Yan Liu, Shuangchi Liu, Andrew Philip Roberts, and Hongmiao Pan. 2020. "Classi Fi Cation of a Complexly Mixed Magnetic Mineral Assemblage in Paci Fi c Ocean Surface Sediment by Electron Microscopy and Supervised Magnetic Unmixing." 8(December):1–18. doi: 10.3389/feart.2020.609058.

Li, Xiaohui, Junbo Yang, Hang Sun, Ling Huang, Hui Li, and Jianping Shi. 2023. "Controlled Synthesis and Accurate Doping of Wafer-Scale 2D Semiconducting Transition Metal Dichalcogenides." *Advanced Materials* 2305115:1–14. doi: 10.1002/adma.202305115.

Lin, Zesen, Changchang Dong, Wei Mu, and Xiaojun Han. 2023. "Degradation of Rhodamine B in the Photocatalytic Reactor Containing TiO2 Nanotube Arrays Coupled with Nanobubbles." *Advanced Sensor and Energy Materials* 2(2):100054. doi: 10.1016/j.asems.2023.100054.

Mahyoub, Samah A., Abdo Hezam, Fahim A. Qaraah, Keerthiraj Namratha, Mysore B. Nayan, Qasem A. Drmosh, Deepalekshmi Ponnamma, and Kullaiah Byrappa. 2021. "Surface Plasmonic Resonance and Z - Scheme Charge Transport Synergy in Three-Dimensional Flower-like Ag − CeO 2 − ZnO Heterostructures for Highly Improved Photocatalytic CO 2 Reduction." doi: 10.1021/acsaem.1c00001.

Malik, Shiza, Khalid Muhammad, and Yasir Waheed. 2023. "Nanotechnology: A Revolution in Modern Industry." *Molecules* 28(2). doi: 10.3390/molecules28020661.

Mirzaeifard, Zahra, Zahra Shariatinia, Milad Jourshabani, and Seyed Mahmood Rezaei Darvishi. 2020. "ZnO Photocatalyst Revisited: Effective Photocatalytic Degradation of Emerging Contaminants Using S-Doped ZnO Nanoparticles under Visible Light Radiation." *Industrial and Engineering Chemistry Research* 59(36):15894–911. doi: 10.1021/acs.iecr.0c03192.

Modwi, Abueliz, Kamal K. Taha, Lotfi Khezami, Mohamed Boudina, Mohamed Khairy, Omer K. Al-Duaij, and Sarra Talab. 2021a. “Dependence of the Electrical Properties of Cu-Doped ZnO Nanoparticles Decorated by Ag Atoms.” *Zeitschrift Für Physikalische Chemie* 235(6):745–67. doi: 10.1515/zpch-2019-1473.

Modwi, Abueliz, Kamal K. Taha, Lotfi Khezami, Mohamed Boudina, Mohamed Khairy, Omer K. Al-Duaij, and Sarra Talab. 2021b. “Dependence of the Electrical Properties of Cu-Doped ZnO Nanoparticles Decorated by Ag Atoms.” *Zeitschrift Fur Physikalische Chemie* 235(6):745–67. doi: 10.1515/zpch-2019-1473.

Nersisyan, Hayk H., Jong Hyeon Lee, Jin-Rui Ding, Kyo-Seon Kim, Khachatur V. Manukyan, and Alexander S. Mukasyan. 2017. “Combustion Synthesis of Zero-, One-, Two- and Three-Dimensional Nanostructures: Current Trends and Future Perspectives.” *Progress in Energy and Combustion Science* 63:79–118. doi: 10.1016/j.pecs.2017.07.002.

Neto, N. F. Andrade, K. N. Matsui, C. A. Paskocimas, M. R. D. Bomio, and F. V Motta. 2019. “Materials Science in Semiconductor Processing Study of the Photocatalysis and Increase of Antimicrobial Properties of Fe 3 + and Pb 2 + Co-Doped ZnO Nanoparticles Obtained by Microwave-Assisted Hydrothermal Method.” *Materials Science in Semiconductor Processing* 93(November 2018):123–33. doi: 10.1016/j.mssp.2018.12.034.

Niu, Feng, Fugong Zhou, Zhixun Wang, Lei Wei, Jie Hu, Lei Dong, Yifei Ma, Mei Wang, Suotang Jia, Xuyuan Chen, and Zhaomin Tong. 2023. “ Synthesizing Metal Oxide Semiconductors on Doped Si/SiO 2 Flexible Fiber Substrates for Wearable Gas Sensing .” *Research* 6:1–9. doi: 10.34133/research.0100.

Ojha, Ankita. 2020. *Nanomaterials for Removal of Waterborne Pathogens*. Elsevier.

Okeil, Sherif, Julian Ungerer, Hermann Nirschl, and Georg Garnweitner. 2024. “Synthesis of Anisotropic Metal Oxide Nanoparticles via Non-Aqueous and Non-Hydrolytic Routes.” *KONA Powder and Particle Journal* 41(41):197–220. doi: 10.14356/kona.2024014.

Ong, Chin Boon, Law Yong Ng, and Abdul Wahab Mohammad. 2018. “A Review of ZnO Nanoparticles as Solar Photocatalysts: Synthesis, Mechanisms and Applications.” *Renewable and Sustainable Energy Reviews* 81(July 2016):536–51. doi:

10.1016/j.rser.2017.08.020.

Osherov, Anna, Ram Prasad, Wojciech Chrzanowski, Elizabeth J. New, Lais Brazaca, Omowunmi Sadik, Christy L. Haynes, and Elicia Maine. 2023. “Responsible Nanotechnology for a Sustainable Future.” *One Earth* 6(7):763–66. doi: 10.1016/j.oneear.2023.06.010.

Pandey, Pramod K., Philip H. Kass, Michelle L. Soupir, Sagor Biswas, and Vijay P. Singh. 2014. “Contamination of Water Resources by Pathogenic Bacteria.” *AMB Express* 4(1):1–16. doi: 10.1186/s13568-014-0051-x.

Pandit, Chetan, Arpita Roy, Suresh Ghotekar, Ameer Khusro, Mohammad Nazmul Islam, Talha Bin Emran, Siok Ee Lam, Mayeen Uddin Khandaker, and David Andrew Bradley. 2022. “Biological Agents for Synthesis of Nanoparticles and Their Applications.” *Journal of King Saud University - Science* 34(3):101869. doi: 10.1016/j.jksus.2022.101869.

Pashchanka, Mikhail, Rudolf C. Hoffmann, Aleksander Gurlo, Janine C. Swarbrick, and Jayaprakash Khanderi. 2011. “PAPER A Molecular Approach to Cu Doped ZnO Nanorods with Tunable Dopant Content.” (June 2016). doi: 10.1039/c0dt01567a.

Pham, Khoa Van. 2020. “A New Method for Assessment of Nickel- Titanium Endodontic Instrument Surface Roughness Using Field Emission Scanning Electronic Microscope.” 1–7.

Piaskowski, Krzysztof, Renata Świderska-Dąbrowska, and Paweł K. Zarzycki. 2018. “Dye Removal from Water and Wastewater Using Various Physical, Chemical, and Biological Processes.” *Journal of AOAC International* 101(5):1371–84. doi: 10.5740/jaoacint.18-0051.

Pop, Oana L., Amalia Mesaros, Dan C. Vodnar, and Ramona Suharoschi. 2020. “Cerium Oxide Nanoparticles and Their E Ffi Cient Antibacterial Application In Vitro against Gram-Positive and Gram-Negative Pathogens.”

Postica, Vasile, Alexander Vahl, David Santos-Carballal, Torben Dankwort, Lorenz Kienle, Mathias Hoppe, Abdelaziz Cadi-Essadek, Nora H. de Leeuw, Maik-Ivo Terasa, Rainer Adelung, Franz Faupel, and Oleg Lupan. 2019. “Tuning ZnO Sensors Reactivity toward Volatile Organic Compounds via Ag Doping and Nanoparticle Functionalization.” *ACS Applied Materials & Interfaces* 11(34):31452–66. doi:

10.1021/acsami.9b07275.

Prasad, Rai Dhirendra, Rai Surendra Prasad, Rai Bishvendra Prasad, Saurabh R. Prasad, Shashi Bhushan Singha, Rai Jitendra Prasad, Pramod Sinha, Sanjay Saxena, Anil Kumar Vaidya, Shivanand. B. B Teli, Umapati Rai Saxena, Avinash Harale, M. B. Deshmukh, M. N. Padvi, and G. J. Navathe. 2024. "A Review on Modern Characterization Techniques for Analysis of Nanomaterials and Biomaterials." *ES Energy & Environment*. doi: 10.30919/esee1087.

Priya, V. Shanmuga, S. Khaleel Basha, and V. Sugantha Kumari. 2023. "Kinetics and Adsorption Performance of Biosorbent Starch / Poly (Vinyl Alcohol)/ Graphene Oxide Nanocomposite for the Removal of Dyes." *Journal of Umm Al-Qura University for Applied Sciences* 9(4):529–47. doi: 10.1007/s43994-023-00063-4.

Qi, Kezhen, Bei Cheng, Jiaguo Yu, and Wingkei Ho. 2017. "Review on the Improvement of the Photocatalytic and Antibacterial Activities of ZnO." *Journal of Alloys and Compounds* 727:792–820. doi: 10.1016/j.jallcom.2017.08.142.

Rabbani, Mahboubeh, Javad Shokraiyan, Rahmatollah Rahimi, and Rezvaneh Amrollahi. 2021. "Comparison of Photocatalytic Activity of ZnO, Ag-ZnO, Cu-ZnO, Ag, Cu-ZnO and TPPS/ZnO for the Degradation of Methylene Blue under UV and Visible Light Irradiation." *Water Science and Technology* 84(7):1813–25. doi: 10.2166/wst.2021.360.

Rafiq, Asma, Muhammad Ikram, S. Ali, Faiza Niaz, Maaz Khan, Qasim Khan, and Muhammad Maqbool. 2021. "Photocatalytic Degradation of Dyes Using Semiconductor Photocatalysts to Clean Industrial Water Pollution." *Journal of Industrial and Engineering Chemistry* 97:111–28. doi: 10.1016/j.jiec.2021.02.017.

Rahman, Mohammed M., Hasan B. Balkhoyor, and Abdullah M. Asiri. 2019. "Removal of a Melamine Contaminant with Ag-Doped ZnO Nanocomposite Materials." *New Journal of Chemistry* 43(47):18848–59. doi: 10.1039/C9NJ04638K.

Rajakumari, S., S. Mohandoss, and S. Sureshkumar. 2023. "Synthesis and Characterization of Cu-RGO/ZnO Nanocomposite for Photocatalytic Degradation of Bromophenol Blue and Antibacterial Activity." *Brazilian Journal of Chemical Engineering* (0123456789). doi: 10.1007/s43153-023-00406-y.

Raju, P., D. Deivatamil, John Abel, Martin Mark, and Joseph Prince. 2022. "Antibacterial

and Catalytic Activity of Cu Doped ZnO Nanoparticles : Structural , Optical , and Morphological Study." *Journal of the Iranian Chemical Society* 19(3):861–72. doi: 10.1007/s13738-021-02352-3.

Rakhsha, Amir Hossein, Hossein Abdizadeh, Erfan Pourshaban, Mohammad Reza Golobostanfard, Valmor Roberto Mastelaro, and Maziar Montazerian. 2019. "Ag and Cu Doped ZnO Nanowires: A PH-Controlled Synthesis via Chemical Bath Deposition." *Materialia* 5:100212. doi: 10.1016/j.mtla.2019.100212.

Ramamoorthy, Raj Kumar, Ezgi Yildirim, Enguerrand Barba, Pierre Roblin, Jorge A. Vargas, Lise-Marie Lacroix, Isaac Rodriguez-Ruiz, Philippe Decorse, Valeri Petkov, Sébastien Teychené, and Guillaume Viau. 2020. "The Role of Pre-Nucleation Clusters in the Crystallization of Gold Nanoparticles." *Nanoscale* 12(30):16173–88. doi: 10.1039/D0NR03486J.

Reali, Savannah, Elias Y. Najib, Krisztina E. Treuerné Balázs, Adeline Chern Hui Tan, Linda Váradi, David E. Hibbs, and Paul W. Groundwater. 2019. "Novel Diagnostics for Point-of-Care Bacterial Detection and Identification." *RSC Advances* 9(37):21486–97. doi: 10.1039/C9RA03118A.

Roduner, Emil. 2006. "Size Matters: Why Nanomaterials Are Different." *Chemical Society Reviews* 35(7):583. doi: 10.1039/b502142c.

Saleh, Tawfik A. 2020. "Nanomaterials: Classification, Properties, and Environmental Toxicities." *Environmental Technology & Innovation* 20:101067. doi: 10.1016/j.eti.2020.101067.

Salem, Salem S. 2023. "A Mini Review on Green Nanotechnology and Its Development in Biological Effects." *Archives of Microbiology* 205(4):1–15. doi: 10.1007/s00203-023-03467-2.

Sarmah, Jumisree, and Arvind Kumar. 2024. "Significance of Using Scanning Electron Microscopy with Energy Dispersive X-Ray Spectrometry (SEM-EDX) for Analysis of Evidence Material in Forensic Sciences." 8(2):1–11. doi: 10.9734/AJR2P/2024/v8i2159.

Schladt, Thomas D., Kerstin Schneider, Hansjörg Schild, and Wolfgang Tremel. 2011. "Synthesis and Bio-Functionalization of Magnetic Nanoparticles for Medical Diagnosis and Treatment." *Dalton Transactions* 40(24):6315–43. doi:

10.1039/c0dt00689k.

Seidel, Michael, Lars Jurzik, Ingrid Brettar, Manfred G. Höfle, and Christian Griebler. 2016. “Microbial and Viral Pathogens in Freshwater: Current Research Aspects Studied in Germany.” *Environmental Earth Sciences* 75(20). doi: 10.1007/s12665-016-6189-x.

Sewnet, Agidew, Esayas Alemayehu, Mulualem Abebe, Dhakshnamoorthy Mani, Sabu Thomas, Nandakumar Kalarikkal, and Bernd Lennartz. 2023. “Single-Step Synthesis of Graphitic Carbon Nitride Nanomaterials by Directly Calcining the Mixture of Urea and Thiourea: Application for Rhodamine B (RhB) Dye Degradation.” *Nanomaterials* 13(4). doi: 10.3390/nano13040762.

Sharma, Sudhendu, P. S. Shera, Rabinder Kaur, and K. S. Sangha. 2016. “Standardization of Egg Dosages for Mass Production of Corcyra Cephalonica (Stainton).” *Phytoparasitica* 44(4):459–64. doi: 10.1007/s12600-016-0542-1.

Shoran, Sachin, Sudesh Chaudhary, and Anshu Sharma. 2022. “Photocatalytic Dye Degradation and Antibacterial Activities of CeO2/g-C3N4 Nanomaterials for Environmental Applications.” *Environmental Science and Pollution Research* 30(44):98682–700. doi: 10.1007/s11356-022-23815-x.

Shrestha, Sweta, Bo Wang, and Prabir Dutta. 2020. “Nanoparticle Processing: Understanding and Controlling Aggregation.” *Advances in Colloid and Interface Science* 279:102162. doi: 10.1016/j.cis.2020.102162.

Silva-neto, Manoel L., Mário C. A. De Oliveira, Christian T. Domingu, Raquel E. M. Lins, Nikifor Rakov, Cid B. De Araújo, and Leonardo De Souza Menezes. 2019. “UV Random Laser Emission from Flexible ZnO-Ag-Enriched Electrospun Cellulose Acetate Fiber Matrix.” (April):1–9. doi: 10.1038/s41598-019-48056-w.

Singh, Shailendra K., Debjit Dutta, Anirban Dhar, Shyamal Das, Mukul C. Paul, and Tarun K. Gangopadhyay. 2019. “Detection of Ammonia Gas Molecules in Aqueous Medium by Using Nanostructured Ag-Doped ZnO Thin Layer Deposited on Modified Clad Optical Fiber.” *Physica Status Solidi (A)* 216(16):1900141. doi: 10.1002/pssa.201900141.

Soltani, Nayereh, Elias Saion, Maryam Erfani, Khadijeh Rezaee, Ghazaleh Bahmanrokh, Gregor P. C. Drummen, Afarin Bahrami, and Mohd Zobir Hussein. 2012. “Influence

of the Polyvinyl Pyrrolidone Concentration on Particle Size and Dispersion of ZnS Nanoparticles Synthesized by Microwave Irradiation." *International Journal of Molecular Sciences* 13(10):12412–27. doi: 10.3390/ijms131012412.

Subash, B., R. Sasikala, K. Jayamoorthy, and P. Magesan. 2023. "Heterojunction of Bentonite Clay Supported Bi 2 O 3 / ZnO Composite for the Detoxification of Azo Dyes under UV-A Light Illumination." *Chemical Physics Impact* 6(November 2022):100152. doi: 10.1016/j.chphi.2022.100152.

Sukhanov, I. I., A. N. Tyumentsev, I. A. Ditenberg, V. M. Chernov, and M. M. Potapenko. 2023. "Thermal Stability of Nanosized Nonmetallic Phase Particles in Low-Activated Dispersion Hardening Vanadium Alloys." 86(7):1577–84. doi: 10.1134/S1063778823070220.

Suresh, R., Lalitha Gnanasekaran, Saravanan Rajendran, Matias Soto-Moscoso, Wei Hsin Chen, Pau Loke Show, and Kuan Shiong Khoo. 2023. "Application of Nanocomposites in Integrated Photocatalytic Techniques for Water Pollution Remediation." *Environmental Technology and Innovation* 31:103149. doi: 10.1016/j.eti.2023.103149.

Tang, Kuok Ho Daniel, Noura M. Darwish, Abdullah M. Alkahtani, Mohamed Ragab AbdelGawwad, and Peter Karácsony. 2022. "Biological Removal of Dyes from Wastewater: A Review of Its Efficiency and Advances." *Tropical Aquatic and Soil Pollution* 2(1):59–75. doi: 10.53623/tasp.v2i1.72.

Tang, Ruikang, Biao Jin, Biao Jin, and Zhaoming Liu. 2020. "Recent Experimental Explorations of Non-Classical Nucleation." *CrystEngComm* 22(24):4057–73. doi: 10.1039/d0ce00480d.

Tavares, T. D., Joana C. Antunes, Jorge Padr, Ana I. Ribeiro, Andrea Zille, M. Teresa P. Amorim, Fernando Ferreira, and Helena P. Felgueiras. 2020. "Activity of Specialized Biomolecules against Gram-Positive and Gram-Negative Bacteria." 1–16.

Thabit, Hammam Abdurabu, Norlaili A. Kabir, Abd Khamim Ismail, and Shoroog Alraddadi. 2022. "Development of Ag-Doped ZnO Thin Films and Thermoluminescence (TLD) Characteristics for Radiation Technology."

Trang, Ton Nu Quynh, Thang Bach Phan, Nguyen Dang Nam, and Vu Thi Hanh Thu. 2020. "In Situ Charge Transfer at the Ag@ZnO Photoelectrochemical Interface

toward the High Photocatalytic Performance of H2 Evolution and RhB Degradation." *ACS Applied Materials and Interfaces* 12(10):12195–206. doi: 10.1021/acsami.9b15578.

De Trizio, Luca, and Liberato Manna. 2016. "Forging Colloidal Nanostructures via Cation Exchange Reactions." *Chemical Reviews* 116(18):10852–87. doi: 10.1021/acs.chemrev.5b00739.

Uma, B., Kurupalya Shivram Anantharaju, B. S. Surendra, K. Gurushantha, Sunil S. More, S. Meena, B. Hemavathi, and H. C. Anand. Murthy. 2023. "Influence of Ag on the Structural, Electrochemical, Antibacterial, and Photocatalytic Performance of the (CuO-Cu2O)Cu Nanocomposite." *ACS Omega* 8(11):9947–61. doi: 10.1021/acsomega.2c07124.

Wang, Shuo, Fuchao Jia, Xiaomei Wang, Leqi Hu, Yuping Sun, Guangchao Yin, Tong Zhou, Zhenyu Feng, Parveen Kumar, and Bo Liu. 2020. "Fabrication of ZnO Nanoparticles Modified by Uniformly Dispersed Ag Nanoparticles: Enhancement of Gas Sensing Performance." *ACS Omega* 5(10):5209–18. doi: 10.1021/acsomega.9b04243.

Wong, Y. C., Y. S. Szeto, W. H. Cheung, and G. McKay. 2004. "Pseudo-First-Order Kinetic Studies of the Sorption of Acid Dyes onto Chitosan." *Journal of Applied Polymer Science* 92(3):1633–45. doi: 10.1002/app.13714.

World Bank Group. 2017. *Drug-Resistant Infections*. Vol. 2. World Bank, Washington, DC.

Xie, Maomao, Meng Gao, Yang Yun, Martin Malmsten, Vincent M. Rotello, and Radek Zboril. 2023. "Antibacterial Nanomaterials : Mechanisms , Impacts on Antimicrobial Angewandte." 202217345. doi: 10.1002/anie.202217345.

Xu, M., Y. Chen, W. Y. Hu, Y. T. Liu, Q. P. Zhang, H. Yuan, X. Y. Wang, J. X. Zhang, K. Y. Luo, J. Li, and G. Xiong. 2020. "Designed Synthesis of Microstructure and Defect-Controlled Cu-Doped ZnO-Ag Nanoparticles: Exploring High-Efficiency Sunlight-Driven Photocatalysts." *Journal of Physics D: Applied Physics* 53(2). doi: 10.1088/1361-6463/ab4bfd.

Xu, M., Y. Chen, W. Y. Hu, Y. T. Liu, Q P Zhang, H. Yuan, X. Y. Wang, J. X. Zhang, K. Y. Luo, J. Li, and G. Xiong. 2020. "Designed Synthesis of Microstructure and Defect-

Controlled Cu-Doped ZnO–Ag Nanoparticles: Exploring High-Efficiency Sunlight-Driven Photocatalysts." *Journal of Physics D: Applied Physics* 53(2):025106. doi: 10.1088/1361-6463/ab4bfd.

Yuan, Lifang, Yahong Jin, Yue Su, Haoyi Wu, Yihua Hu, and Shihe Yang. 2020. "Optically Stimulated Luminescence Phosphors : Principles , Applications , and Prospects." 2000123:1–34. doi: 10.1002/lpor.202000123.

Zeng, Leli, B. H. Jaswant. Gowda, Mohammed Gulzar Ahmed, Mohammed A. S. Abourehab, Zhe Sheng Chen, Changhua Zhang, Jia Li, and Prashant Kesharwani. 2023. "Advancements in Nanoparticle-Based Treatment Approaches for Skin Cancer Therapy." *Molecular Cancer* 22(1):1–50. doi: 10.1186/s12943-022-01708-4.

Zhang, Yi, Xingjie Gao, Lei Zhi, Xin Liu, Wei Jiang, Yanhua Sun, and Jie Yang. 2014. "The Synergetic Antibacterial Activity of Ag Islands on ZnO (Ag/ZnO) Heterostructure Nanoparticles and Its Mode of Action." *Journal of Inorganic Biochemistry* 130(1):74–83. doi: 10.1016/j.jinorgbio.2013.10.004.

Zulkiflee, A., Mohammad Mansoob Khan, Abuzar Khan, Aniz Chennampilly Ummer, Mohammad Hilni Harunsani, and Mohd Yusuf Khan. 2023. "Zirconium-Doped BiOCl for Enhanced Visible Light-Induced Photocatalytic Degradation of RhB Dye and Photoelectrochemical Studies." doi: 10.1039/d3nj02294c.